HHS Public Access

Author manuscript

Nature. Author manuscript; available in PMC 2016 November 04.

Published in final edited form as:

Nature. ; 533: 206–211. doi:10.1038/nature17977.

Sex-specific pruning of neuronal synapses in *Caenorhabditis elegans*

Meital Oren-Suissa, **Emily A. Bayer**, and **Oliver Hobert**

Department of Biology, Department of Biochemistry and Molecular Biophysics, Columbia University, Howard Hughes Medical Institute, New York, USA

Meital Oren-Suissa: meitals@gmail.com; Oliver Hobert: or38@columbia.edu

Abstract

Whether and how neurons that are present in both sexes of the same species can differentiate in a sexually dimorphic manner is not well understood. A comparison of the connectomes of the *Caenorhabditis elegans* hermaphrodite and male nervous systems reveals the existence of sexually dimorphic synaptic connections between neurons present in both sexes. Here, we demonstrate sex-specific functions of these sex-shared neurons and show that many neurons initially form synapses in a hybrid manner in both the male and hermaphrodite pattern before sexual maturation. Sex-specific synapse pruning then results in the sex-specific maintenance of subsets of the connections. Reversal of the sexual identity of either the pre- or postsynaptic neuron alone transforms the patterns of synaptic connectivity to that of the opposite sex. A dimorphically expressed and phylogenetically conserved transcription factor is both necessary and sufficient to determine sex-specific connectivity patterns. Our studies reveal new insights into sex-specific circuit development.

Like other invertebrate or vertebrate nervous systems, the nervous system of *C. elegans* contains a number of sex-specific neurons, most of which are generated during the process of sexual maturation in late larval stages. Apart from these sex-specific neurons (8 in hermaphrodites, 91 in males), there are 294 neurons shared by both sexes, most of which embryonically generated[1,2]. The hermaphrodite and male versions of these shared neurons display the same lineage history, the same cell body position, share molecular features (e.g. neurotransmitter identity) and display similar neurite projection patterns [1,3–5]. Intriguingly, the recent reconstruction of the posterior nervous system of the *C. elegans* adult male[3] and its comparison to the connectome of the hermaphrodite (a derived female) [6] shows that several of the sex-shared neurons are strongly sexually dimorphic in their synaptic wiring

Correspondence and requests for materials should be addressed to M.O. (meitals@gmail.com) or O.H. (or38@columbia.edu)..

AUTHOR CONTRIBUTIONS

M.O. and O.H. designed the experiments. M.O. performed most experiments. E.A.B. quantified the data for PHA-AVG synapses and all iBLINC transgenes, tracked silenced PHB animals and generated driver lines for expression analysis of *gpa-6* and *flp-18*. M.O. and O.H. wrote the paper with input from E.A.B.

AUTHOR INFORMATION

The authors declare no competing financial interests. Readers are welcome to comment on the online version of the paper.

patterns. These anatomical observations provide a fascinating opportunity to study the question of how seemingly similar sex-shared neurons develop sexually dimorphic characteristics.

Sexually dimorphic synaptic target choices between sex-shared neurons

Here, we focus on a group of sex-shared, but dimorphically connected sensory, inter- and motorneurons (Fig. 1a)[3]. The sexually dimorphic connectivity differences do not simply reflect sex-specific modifications of similar neuronal circuits, but sex-shared neurons rather wire into completely distinct circuits (Fig. 1a)[3]. For example, the PHB phasmid sensory neuron synapses onto three different, sex-shared command interneurons only in hermaphrodites (AVA, AVD and PVC). In males, PHB rather connects to a sex-shared interneuron, AVG which in turns connects to downstream motor neurons again only in males (Fig. 1a). To examine whether dimorphic connections are due to dimorphic synaptic partner choice or a reflection of sex-specific neuron or process placement, we analyzed serial electron micrographs and found that the PHA and PHB phasmid neuron processes are directly adjacent to the AVG process in both sexes (Extended Data Fig. 1). Dimorphic connections between these neurons are therefore a consequence of sex-specific synaptic partner choice.

While EM provides a powerful tool to identify synaptic partners, the presently available EM analysis relies on one or two animals at a single stage (adult). To confirm the EM results, and to visualize the reproducibility as well as the developmental aspects of dimorphic synapses, we used two distinct transsynaptic labeling techniques (Fig. 1c), “GRASP” (“GFP Reconstitution Across Synaptic Partners”)[7] and “iBLINC” (in vivo Biotin Labeling of INtercellular Contact)[8]. We generated transgenic lines in which seven distinct synaptically connected neuron pairs are labeled with GRASP and/or iBLINC (Fig. 1b; Extended Data Fig. 2,Fig. 3). Using cytosolic mCherry to label neurites, we examined synaptic puncta along these mCherry-labeled, adjacent processes. For all seven synaptic connections examined, we identified discrete synaptic puncta that appear in the sexually dimorphic manner predicted by the EM analysis (Fig. 1a,b; Extended Data Fig. 1,Fig. 3).

Sexually dimorphic functions of sex-shared neurons

To assess whether sexually dimorphic wiring is an indication of dimorphic neuronal function, we either surgically removed individual, dimorphically connected neurons or genetically silenced them using ectopic expression of a histamine-gated chloride channel [9]. Silencing of the PHB neurons (using a driver that is strongly and consistently expressed only in PHB; Extended Data Fig. 4) affected forward locomotion of hermaphrodites, but not of males (Extended Data Fig. 5a). Another, previously described PHB function, also displays striking sex-specificity. Specifically, it has been shown that the PHB sensory neuron modulates chemorepulsive behavior of hermaphrodites in response to the noxious chemical SDS[10]. The modulatory effect of PHB is observed upon functionally disabling subsets of head sensory neurons[10]. Such head neuron-defective animals fail to avoid SDS because PHB provides an antagonistic input to command interneurons[10]. This antagonistic input to the command circuit is revealed through ablation of PHB, which restores the ability of head

sensory-neuron defective animals to avoid SDS[10]. We corroborated this antagonistic input through silencing of PHB with a histamine-gated chloride channel, by examining *ceh-14* mutant animals, in which all three phasmid neurons fail to adopt their glutamatergic identity [11], and by silencing both ASH and PHB neurons (Fig. 2a; Extended Data Fig. 5d–e). Importantly, male PHB does not connect to command interneurons and no antagonistic input to the command circuit is expected. One would therefore predict that the disabling of head sensory-neuron function in males (ASH silenced and ablated; or *tax-4* mutants) should not have the impact on SDS avoidance that is observed in hermaphrodites. We indeed found this to be the case (Fig. 2a; Extended Data Fig. 5).

If male PHB neurons are not involved in the avoidance of noxious chemicals, what function do they adopt in males? We noted that the male-specific innervation target of PHB, the interneuron AVG, becomes innervated by male-specific hook sensory neurons (HOA and HOB), known to be involved in sensing a hermaphrodite-derived signal that induces males to stop at the vulva during mating behavior[12]. Moreover, PHB also innervates HOA directly[3]. Through genetic silencing, genetic ablation and microsurgical laser ablations, we found that PHB and AVG are involved in responding to this vulva stop signal (Fig. 2b,c). Ablation of VD13, one of the motor neurons innervated by AVG specifically in males also causes vulva location defects (Fig. 2c) and so does ablation of the LUA neuron (Extended Data Fig. 6). PHB also innervates the male-specific PVX and PVY neurons, involved in mate contact-induced backward locomotion in males [13] and silencing PHB affects this sexually dimorphic behavior as well (Fig. 2d). We conclude that PHB has sexually dimorphic functions, modulating locomotion and processing repulsive environmental sensory information in hermaphrodites while sensing hermaphrodite-derived mating cues in males (summarized in Extended Data Fig. 6c).

Sex-shared, interneurons also display sexually dimorphic functions. We found that the dimorphically connected LUA neuron is also involved in response to vulva stop signal in males, while automated worm-tracking analysis [14] revealed that ablation of LUAs results in pausing defects in hermaphrodites but not in males (Extended Data Fig. 6).

Sexually dimorphic synapses are formed by pruning or are prepatterned

We next asked how sexually dimorphic connectivity patterns are established. With the exception of the VD13 neuron (which is born at the end of the first larval stage[15]), the shared neurons that we analyzed are born and project their neurites during embryogenesis. Sex-specific neurons in the tail are born in the last larval stage[16] and male-specific behaviors emerge soon after[17]. One could therefore envision that dimorphic connections between the embryonically born neurons could form during sexual maturation, i.e. long after the respective neurons and axonal patterns have been established in the animal (“late maturation” model; Fig. 3a). Alternatively, a “default connectivity” could be established by both sexes early in development, followed by a sex-specific synapse rewiring upon sexual maturation (“rewiring” model; Fig. 3a). By analyzing connectivity throughout larval development using the GRASP and iBLINC systems, we discovered two different mechanisms – a “pruning” mechanism, used by many different neurons, and a “prepatterning” mechanism used by others (Fig. 3a).

For example, PHB neurons connect to AVA and AVG in hermaphrodites and males at early larval stages (Fig. 3b,c). Therefore, male-specific pruning of the PHB>AVA synapses results in an adult male-specific PHB>AVG connection, and conversely, hermaphrodite-specific pruning of the PHB>AVG synapses results in the hermaphrodite specific PHB>AVA synapses. We observed these synaptic pruning events to occur during sexual maturation in the fourth larval stage (L4) (Extended Data Fig. 7).

Since the PHB>AVA connection exists in both sexes at the L1 stage, we asked whether at this stage both hermaphrodites and males display a PHB-dependent modulation of the repulsive response to noxious chemicals. We indeed found this to be the case (Fig. 2a). The repulsive response was restored in both sexes upon silencing of PHB (Extended Data Fig. 5f). These observations demonstrate that PHB does not merely acquire dimorphic functions in the adult, but that in males, PHB neurons undergo a repurposing of function, from initially being involved in sensing noxious environmental cues to processing sex-specific cues.

Sexually dimorphic pruning of synaptic connections can also be observed in a number of additional neuronal contexts (Fig. 3; Extended Data Fig. 2). For example, PHA connects to AVG in both sexes at the L1 stage, but this connection is selectively lost in males (Fig. 3b–c). Similarly, the AVG interneuron connects to the cholinergic DA9 motor neuron in both sexes at the L1 stage, but the synaptic connection persists only in males, not hermaphrodites (Fig. 1d, Fig. 3b–c).

One other sexually dimorphic synaptic connection arises by a fundamentally different principle: The AVG to VD13 connection is only ever observed in males, and never in hermaphrodites (Fig. 1d, Fig. 3b–c). Some prepatterning is also already evident in the pruned AVG>DA9 synapses; these are present in both sexes in the L1 stage, but are stronger in the male (Fig. 3b–c). Analysis of ~1,000 serial EM sections shows that the axons of the AVG and VD13 (synaptically connected in a male-specific manner) are more adjacent in males compared to hermaphrodites (Extended Data Fig. 1). Even though we cannot exclude the possibility that dimorphic adjacency is a mere secondary consequence of failure to establish synaptic contact, we propose that the prepatterning of dimorphic synapse may be a consequence of dimorphic axon placement. Taken together, we identified two types of synaptic maturation events pruning events that coincide with sexual maturation and dimorphic prepatterning events that precede sexual maturation (summarized in Fig. 3d).

The sex of either pre- or postsynaptic neuron controls synaptic patterning

Are sexually dimorphic wiring patterns determined by the sex of both the pre- and post-synaptic cell or perhaps by non cell-autonomous processes? We addressed this question by generating sexually mosaic animals through cell-type specific, ectopic expression of the *fem-3* gene, which downregulates the global, hermaphroditic identity determinant TRA-1, a Gli-type Zn finger transcription factor, thereby imposing a male identity on the specific cell type in an otherwise hermaphroditic animal[4,18,19]. Conversely, ectopic, cell-type specific expression of the intracellular domain of the TRA-2 receptor ("TRA-2^{IC}") feminizes cells via stabilization of the TRA-1 transcription factor in otherwise male animals[17,20]. We found that identity transformations of single neurons transformed synaptic wiring patterns to that

of the opposite sex (Fig. 4; Extended Data Fig. 8). For example, masculinization of PHB results in a loss of the PHB>AVA connection in an otherwise hermaphroditic animal and a gain of the PHB>AVG connection, demonstrating that the sex of PHB dictates which connection is pruned or maintained. Non-dimorphic PHB connectivity at the L1 stage is not affected by sex-reversal (Extended Data Fig. 8). Notably, masculinization of PHB also restores the behavioral defects of head sensory neuron-disabled hermaphrodites (Fig. 2a). Thus, the behavioral differences between males and hermaphrodites in the noxious chemical response can be linked specifically to the sex of an individual neuron (Fig. 2).

Not only is the sex of the presynaptic neuron a determinant of sex-specific wiring patterns, but the postsynaptic cell is also important for establishing proper connectivity (Fig. 4). Masculinization of AVG in hermaphrodites (in which PHB does not normally connect to AVG) will now maintain the PHB>AVG connection. Similarly, masculinization of AVA disrupts maintenance of the PHB>AVA synapses in hermaphrodites (Fig. 4).

Feminizing neurons cell-autonomously via expression of TRA-2^{IC}, in otherwise male animals generally produced the converse effects (Fig. 4). For example, feminization of the PHB neurons in male animals is sufficient to maintain the normally hermaphrodite-specific PHB>AVA synapse and prune the normally male-specific PHB>AVG synapses (Fig. 4). These ectopic PHB>AVA synapses seem to be functional, as *tax-4* males with feminized PHBs reverse less and can antagonize the SDS response (Fig. 2a).

We further probed the non-autonomous nature of maintaining sex-specific synapses by asking whether the maintenance of the PHB>AVG synapse in hermaphrodites through masculinization of AVG, will impact on the maintenance of the hermaphrodite-specific PHB>AVA synapse. Indeed, in animals in which *fem-3* is driven in AVG (resulting in stabilization of the PHB>AVG synapse), PHB>AVA synapse number is significantly reduced. Conversely, in hermaphrodites, in which we masculinized AVA, the PHB>AVA synapse is not only pruned, but the PHB>AVG is now stabilized (Fig. 4). These results suggest a competition mechanism in which one synaptic wiring configuration is maintained on the expense of the “alternative” wiring pattern.

Doublesex-like transcription factors control dimorphic connectivity

What is the link between the globally-acting sex determination system, mediated by TRA-1, and synaptic pruning? A recently framed hypothesis posits that globally-acting hormonal signals in vertebrates operate through region-specific, modular effector system[21]. In *C. elegans*, the global TRA-1 regulator may operate in a cell-type specific manner through one of the 11 members of the DMD (“Doublesex/MAB-3 domain”) family of transcription factors, which are conserved regulators of sexual identity in various organisms[22]. Three of these family members (*mab-3, mab-23, dmd-3*) have previously been implicated in somatic sex differences[4], but the other eight have remained uncharacterized so far. We found that *dmd-5* and *dmd-11* are dimorphically expressed in the dimorphically connected AVG neuron described above; expression is observed in male AVG, but not in hermaphrodite AVG (Fig. 5a). This dimorphic expression is controlled cell-autonomously via the canonical sex-determination pathway and TRA-1, since expression of FEM-3, the negative regulator of

hermaphroditic TRA-1 protein, in the AVG neurons derepresses *dmd-5* and *dmd-11* expression in the AVG neurons of hermaphrodites (Fig. 5a and Extended Data Fig. 9a).

dmd-5 and *dmd-11* single mutants show defects in the male-specific function of AVG in mating behavior (Fig. 5b and Extended Data Fig. 9f–h) and *dmd-5; dmd-11* double mutant animals show even stronger defects (Fig. 5b). These defects can be rescued by AVG-specific expression of either *dmd-5* or *dmd-11* (Fig. 5b). Moreover, *dmd-5* single mutants and *dmd-5; dmd-11* double mutants display the alterations in AVG synaptic wiring that one would expect from factors that control the sexually dimorphic nature of AVG wiring (Fig. 5c–d; Extended Data Fig. 9). Male-specific PHB>AVG synapses fail to be maintained in *dmd-5; dmd-11* mutant males. Synaptic defects can be rescued through AVG-specific expression of *dmd-5* (Fig. 5c–d). There are no synaptic defects observed in the L1 stage of *dmd-5; dmd-11* mutants when no synaptic dimorphism is yet apparent (Extended Data Fig. 9b), indicating that *dmd-5/11* are not required for synapse formation *per se*, but are specifically involved in controlling sex-specific synapse maintenance by preventing synaptic pruning, as predicted by their expression pattern. Furthermore, the PHB>AVA hermaphroditic connection is non-autonomously stabilized in *dmd-5; dmd-11* mutant males, supporting the competition model discussed above (Extended Data Fig. 9e).

dmd-5 is not only required but also sufficient to prevent synaptic pruning, as deduced by ectopic *dmd-5* expression in the AVG neurons of hermaphrodites. In these animals the PHB>AVG synapses are now maintained (Fig. 5d). Since DMD proteins are generally thought to work as repressors[22], we propose that *dmd-5*, in conjunction with *dmd-11*, represses the expression of gene(s) in male AVG neurons that are involved in the pruning of AVG's connections to PHB and that repression of these pruning factor(s) in hermaphroditic AVG, via ectopic *dmd-5* expression, inhibits pruning (summarized in Extended Data Fig. 9j). Notably, while AVG-masculinized *dmd-5(+)* hermaphrodites (masculinized through *fem-3* driven degradation of TRA-1) do maintain PHB>AVG synapses, AVG-masculinized *dmd-5(−)* hermaphrodites do not (Fig. 5d, Extended Data Fig. 9d). This demonstrates that *dmd-5* functions downstream of *tra-1*, as already suggested by the observation of ectopic *dmd-5* expression in animals in which we degraded TRA-1 cell-autonomously in AVG (see above; Fig. 5a and Extended Data Fig. 9a).

In conclusion, our studies show how sex-shared neurons adopt sex-specific synaptic wiring patterns. Sex-specific wiring patterns arise in a neuron-type specific manner. In most cases, we observe sexual maturation-coupled, sex-specific pruning of synaptic connections that were indiscriminately generated in both sexes. In at least one case, sex-specific synapses are pre-patterned before overt sexual maturation of the animal. We observed striking patterns of cellular autonomy of the synaptic pruning events and we found pruning to be regulated by sex-specifically expressed transcription factors.

METHODS

C. elegans strains

Wild-type strains were *C. elegans* variety Bristol, strain N2. Worms were maintained according to standard methods [24]. Worms were grown at 20°C on nematode growth media

(NGM) plates seeded with bacteria (*E.coli* OP50) as a food source. Mutant strains used in this study include:

CB1489 *him-8(e1489) IV*

CB4088 *him-5(e1490) V*

MT633 *lin-11(n389) I; him-5(e1467) V*

RB1295 *F10C1.5(ok1394)/+ II*

FX01760 *dmd-5(tm1760)/+ II*

PR678 *tax-4(p678) III*

DA509 *unc-31(e928) IV*

TB528 *ceh-14(ch3) X*

VC30074 *dmd-5(gk408945) II*

VC1193 *dmd-11(gk552) V*

All transgenic used in this study are listed in Supplementary Table 1, ordered by Figures and Extended Figures.

Cloning and constructs

To generate *inx-18p::wCherry (pMO10)*, *inx-18* second intron was amplified from *pOH260* [25] and restriction sites were added to ends (5' SphI, 3' PstI). This fragment was digested and ligated into *pPD95.75* vector in which the GFP was replaced with codon-optimized mCherry ("worm Cherry"). To restrict expression to AVG, AIY motif (ATTAGTTTCGTTAA) was deleted from the 2nd intron of *inx-18* using site directed mutagenesis (Forward primer: aatttttttcatgttacctacttatttttttctattagcgtcatagat, Reverse: atctatgacgctaatagaaaaaaaataa gtaggtaacatgaaaaaaaatt). *inx-18* 2nd intron is also dimly and variably expressed in URX.

FEM-3::SL2 was amplified from *P(rab-3)::FEM-3::SL2::mCherry* Gateway construct[18] using PCR and KpnI restriction site was added to 5' end. This PCR was digested and inserted into KpnI; AscI digested *pPD95.75* with wCherry, to generate *FEM-3::SL2::wCherry (pMO11)*.

To generate *inx-18::FEM-3::SL2::wCherry (pMO12), pMO10* was digested using SphI, PstI and ligated into digested *pMO11*.

To generate *inx-18::NLG-1::GFP1–10 (pMO17), inx-18::NLG-1::GFP11 (pMO18), inx-18::BirA::NRX-1 (pMO19)* and *inx-18::AP::NLG-1 (pMO24)*, *inx-18p* was cloned from *pMO10 (inx-18p::wCherry)* into the SphI, XmaI sites of MVC2 (*pSM::nlg-1::GFP1–10*), *MVC3 (pSM::nlg-1::GFP11)* (Kind gift from Miri VanHoven), pgcy-8::BirA::NRX-1 and pttx-3::AP::NLG-1 (Kind gift from Hannes Bulow), respectively.

eat-4p9 ("LUA promoter", a fragment of 172 bp upstream to the *eat-4* gene) was amplified using PCR from *eat-4p2* [11] and restriction sites were added to ends (5' HindIII, 3' BamHI).

This fragment was digested and ligated into *pPD95.75* vector, to generate *eat-4p9::GFP (pMO13). eat-4p9* is expressed in the tail neurons LUAs and PVR.

To generate *eat-4p9::NLG-1::GFP1–10 (pMO14)*, *eat-4p9* was amplified from *eat-4p2* and restriction sites were added to ends (5' XbaI, 3' NheI). This fragment was digested and ligated into *MVC2*.

To generate *eat-4p9::FEM-3::SL2::wCherry (pMO15), pMO14* was digested using SpeI, NheI and the fragment containing *eat-4p9* was ligated into *pMO11*.

eat-4p9::wCherry was generated by PCR fusion of *eat-4p9* and *wCherry* [26].

To generate *eat-4p9::BirA::NRX-1 (pMO16)*, *eat-4p9* was amplified from *eat-4p2* and restriction sites were added (5' XmaI, 3' SphI). This fragment was digested and ligated into *digested pgcy-8::BirA::NRX-1*.

To generate *gpa-6::NLG-1::GFP11 (pMO21), gpa-6::BirA::NRX-1 (pMO22)* and *gpa-6::FEM-3::SL2::wCherry (pMO29)*, 2.6kb *gpa-6* promoter was cloned from *MVC6* (*pSM::gpa-6::NLG-1::GFP1–10*, kind gift from Miri VanHoven) into the SphI, SmaI sites of MVC3 (*pSM::nlg-1::GFP11*), *pgcy8-BirA-nrx1* and *pMO11*, respectively. To generate *gpa-6p::GFP* the 2.6kb *gpa-6* fragment was cloned into the SphI, SmaI sites of pPD95.75. *gpa-6* is expressed brightly and consistently in PHBs and also dimly and variably in AWAs.

To generate *flp-18p::FEM-3::SL2::2XNLS::TagRFP (pMO30)*, FEM-3 was cloned into an SL2::2xNLS::TagRFP plasmid using RF cloning [27]. 3.1kb *flp-18* PCR product was cloned into the SphI, XmaI sites of *FEM-3::SL2::2XNLS::TagRFP*. To generate *flp-18p::GFP* the 3.1kb *flp-18* PCR product was cloned into the SphI, XmaI sites of pPD95.75. *flp-18* is expressed brightly and consistently in AVAs and dimly and variably in AIYs.

To generate *srg-13::BirA::NRX-1 (pMO23)*, a 3kb promoter fragment of srg-13 was amplified from genomic DNA (primer F; GTACCTGCAGAAGGACTTGG CAGAAAGAAGC, R: TGCACCCGGGGTGGGCTGTAATTTTTAGCTCG), with PstI, XmaI sites added to ends. This was cloned into the PstI, XmaI sites of pPD95.75. A 2.2Kb *srg-13* promoter was then cloned into the SphI, XmaI sites of *pgcy-8::BirA::NRX-1*.

To generate *acr-2::AP::NLG-1 (pMO25), acr-2p* was cloned from *pEVL194* (*acr-2::NLG-1::GFP11*, kind gift from Brian D. Ackley) into the SphI, XmaI sites of pttx-3::AP::NLG-1.

To generate the cell specific feminizing constructs, *TRA-2(ic)::SL2::2xNLS::TagRFP (pMO37)* was made by inserting *tra-2(ic)* from pENTRY 1–2 tra-2 (ic) (a kind gift from Douglas Portman) into an *SL2::2xNLS::TagRFP* construct using RF cloning. *inx-18::TRA-2(ic)::SL2::2xNLS::TagRFP (pMO32) was* generated by subcloning *inx-18p* from *pMO10 (inx-18p::wCherry)* into the SphI, XmaI sites of *pMO37*. *gpa-6::TRA-2(ic)::SL2::2xNLS::TagRFP (pMO33)* was generated by subcloning *gpa-6* promoter from *MVC6* into the SphI, SmaI sites of *pMO37*. *flp-18::TRA-2(ic)::SL2::2xNLS::TagRFP (pMO34)* was generated by subcloning 3.1kb *flp-18* PCR product from MVC 12 into the SphI, XmaI sites of *pMO37*.

eat-4p9::TRA-2(ic)::SL2::2xNLS::TagRFP was generated by ligating the digested *eat-4p9* mentioned above into the SphI, XmaI sites of *pMO37*.

To generate PHB histamine induced silencing construct, 2.6kb *gpa-6* promoter from MVC6 was cloned into *pNP403* (*tag-168::HisCl1::SL2::GFP*, kind gift from Navin Pokala and Cori Bargmann) to replace the *tag-168* promoter using RF cloning.

To generate *dmd-5* and *dmd-11* genomic rescue constructs, *dmd-5* and *dmd-11* genomic sequences including 500bp 3'UTR were amplified from genomic DNA and cloned into *pMO10* to replace wCherry using RF cloning. The resulting constructs are *pMO31*, *inx-18p::dmd-5_genomic+3'UTR* and *pMO38*, *inx-18p::dmd-11_genomic+3'UTR*.

Microscopy

Worms were anesthetized using 100mM of sodium azide (NaN3) and mounted on 5% agar on glass slides. Worms were analyzed by Nomarski optics and fluorescence microscopy, using a Zeiss 780 confocal laser-scanning microscope. When using GFP, we estimated the resolution of our confocal to be ~250 nm. Multidimensional data was reconstructed as maximum intensity projections using Zeiss Zen software. Puncta were quantified by scanning the original full Z-stack for distinct dots in the area where the processes of the two neurons overlap. Figures were prepared using Adobe Photoshop CS6 and Adobe Illustrator CS6.

Cell ablation

We performed laser ablations using a MicroPoint Laser System Basic Unit (N2 pulsed laser (dye pump), ANDOR Technology) attached to a Zeiss Axioplan 2IE widefield microscope (Objective EC Plan-Neofluar 100×/1.30 Oil M27). This laser delivers 120 μJoules of 337 nm energy with a 3 nsec pulse length. Ablations were done as previously described [34], with pulse repetition rates ~ 15 Hz. Cell identification was done with a GFP or Cherry markers. Ablations were performed at the L4 stage, and worms were analyzed 24–48 hours later. Mock animals were placed on same slide under microscope but were not ablated, and were allowed to recover in a similar manner. After relevant assays were performed (tracking or mating assays), worms were mounted again on glass slides and analyzed under microscope to validate that cell-ablation was successful.

Mating behavior assays

Mating assays were based on procedures described previously [12,35]. Males were picked at an early L4 stage and kept apart from hermaphrodites for 24 hours. One male was transferred to a plate covered with a thin fresh OP50 lawn containing 10–15 adult *unc-31(e928)* hermaphrodites. These hermaphrodites move very little, allowing for an easy recording of male behavior. Hermaphrodites were also isolated from opposite sex at the L4 stage and used 24 hours later. Animals were monitored and sequence of events was recorded within a 15 min window or until the male ejaculated, whichever occurred first. Males were tested for their ability to locate vulva in a mating assay, calculated as location efficiency (L.E.)[36]. The number of passes or hesitations at the vulva until the male first stops at the vulva were counted. Location Efficiency = 1 / # encounters to stop. PHB silenced males were digitally

recorded using the Exo Labs model 1 camera mounted on Nikon Eclipse E400 compound microscope with long-distance X20 lenses. These videos were analyzed for vulva location efficiency and % of successful contact response, which requires tail apposition and initiation of backward locomotion. % response to contact = 100x [the number of times a male exhibited contact response/the number of times the male makes contact with a hermaphrodite via the rays[13].

SDS-avoidance behavior

SDS avoidance assay was based on procedures described previously [10]. A small drop of solution containing either the repellent (0.1% SDS in M13 buffer) or buffer (M13 buffer: 30 mM Tris-HCl pH 7.0, 100 mM NaCl, 10 mM KCl) is delivered near the tail of an animal while it moves forward. Once in contact with the tail, the drop surrounds the entire animal by capillary action and reaches the anterior amphid sensory organs. Drop was delivered using 10 µl glass calibrated pipets (VWR international) pulled by hand on a flame to reduce the diameter of the tip. The capillary pipette was mounted in a holder with rubber tubing and operated by mouth. Assayed worms were transferred to fresh non-wet unseeded NGM plates and allowed to rest at room temp for a few minutes. Each assayed started with testing the animals with drops of buffer alone. The response to each drop was scored as reversing or not reversing. The avoidance index is the number of reversal responses divided by the total number of trials. An Inter Stimuli Interval of at least two minutes was used between successive drops to the same animal. Each animal was tested at least 10 times. The L1 animals were scored blindly and sex was noted 48 hr later.

Neuronal silencing using the histamine chloride channel 1 (HisCl1) system

ASH::HisCl1 (kyEx5104), PHBp::HisCl1 (otEx6341), PHBp::HisCl1; tax-4(p678) and *ASH::HisCl1; PHBp::HisCl1* transgenic animals were picked at the L4 stage and placed on NGM plates containing 10mM histamine with OP50 bacteria as food source. As a control, animals were placed on NGM plates containing OP50 bacteria but no histamine. Chemorepulsion behavior assays were performed 24 hours later. Histamine plates were prepared as previously described [37]. As additional controls, pan-neural *HisCl1* transgenic worms (*CX14373 kyEx4571 [pNP403 (tag-168::HisCl1::SL2::GFP), myo-3::mCherry]*, a kind gift from Cori Bargmann) were placed on Histamine plates prior to use and the time until worm paralysis was measured. Wild-type worms were analyzed on histamine plates and no changes were observed from animals analyzed on non-histamine plates.

Automatic worm tracking

Hermaphrodite and male transgenic otIs462 animals were ablated at the L4 stage and left to recover for 24 hours before tracking. PHB silenced hermaphrodites and males were transferred into NGM plates containing 10mM histamine for 24 hours before tracking. At the adult stage animals were placed on an NGM plate seeded with diluted 20 µl of OP50 bacteria in the center. As a control, mock ablated transgenic otIs462 animals were used. Automatic tracking was performed at ~ 22°C (room temperature) with Worm Tracker 2.0 (WT2), which uses a mobile camera to track and record individual worms and 5 min videos were generated. Analysis of the tracking videos was performed as previously described [14].

To assess the effect of LUA ablation, we first conducted a pilot tracking study of LUA-ablated hermaphrodites worms versus controls and LUA-ablated males versus controls. Due to the extensive analysis of the tracking system, 702 features were initially measured. After correction for multiple testing, pausing and pausing-related features emerged as the main, significant difference between LUA-ablated males and hermaphrodites. Therefore, to obviate further heavy corrections for multiple testing, we chose to re-run these experiments, this time only measuring pausing, permitting us to use of the uncorrected p-value. Within this subset of new experiments, wherein only 1 feature was measured (i.e., pausing), we found highly significant p-values. Given the necessity of 4 tests to make the proof, we chose the most conservative correction possible for multiple testing, Bonferroni, to illustrate that the p-values measured maintain significance even after such extreme correction.

Analysis of EM data

Original TEM serial electron micrographs from “JSE” hermaphrodite tail series and “N2Y” male tail series were analyzed using Elegance software [38].

Images were aligned and screened for adjacency of neuronal processes of the pairs of cells described in this manuscript. For JSE, images from “PAG” and “red series” were analyzed, and for N2Y PAG images were analyzed.

Extended Data

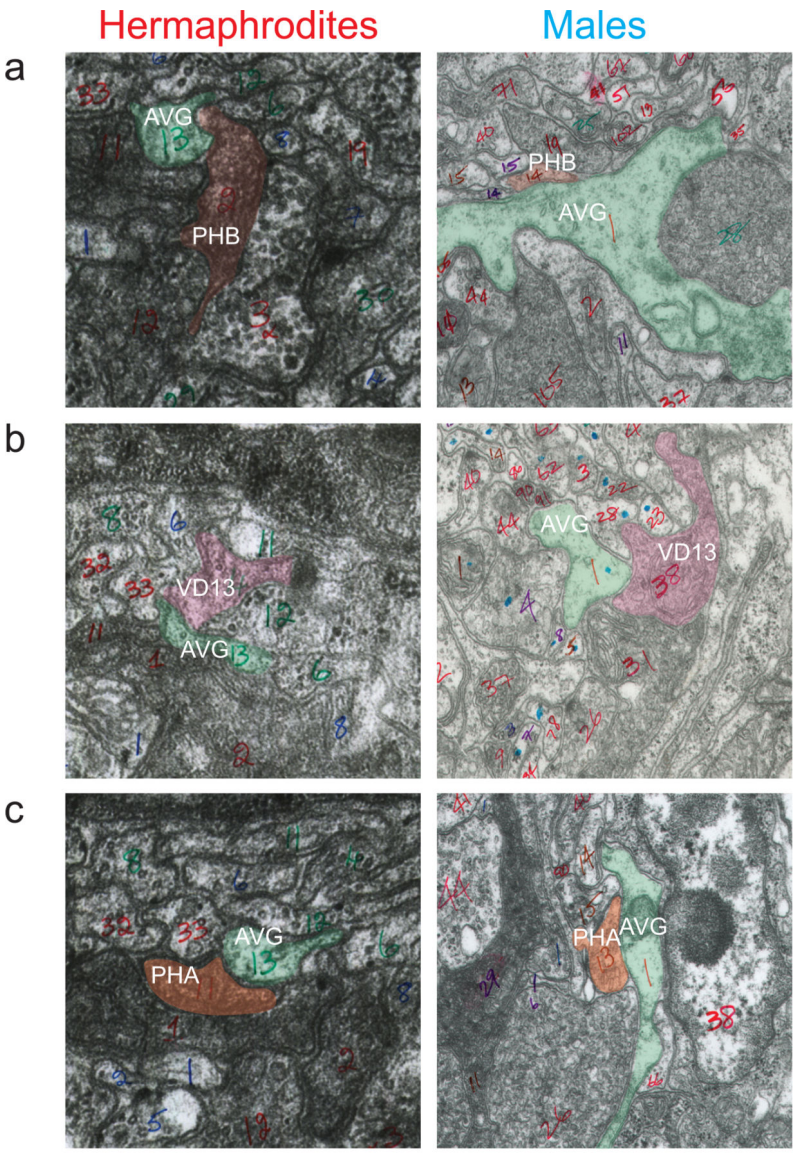

d

Synapses	Sex-specific connection	# sections processes are adjacent	
		Hermaphrodite	Male
PHB>AVG	M	123	206
AVG>VD13	M	14	193
PHA>AVG	H	198	285

Extended Data Figure 1. Adjacency of neuronal processes in hermaphrodites and males

Four TEM prints from wild-type adult hermaphrodite "JSE" [6] and four from adult male "N2Y", showing adjacency of neuronal processes. Tthese images were collected at MRC/LMB for Ref.6 and Ref.16, and the annotated images are now available online at www.wormimage.org, courtesy of David Hall. The set of processes directly adjacent to one another has been defined as the "neighborhood" of that process [39], and the placement of

processes into specific neighborhoods is a major determinant of connectivity. Connections form only in one sex, although processes are adjacent in both sexes.

a: Print #385, JSE series (JSE_122283), http://wormimage.org/image.php?id=122283&page=2 and print #620, N2Y series (PAG620), http://wormimage.org/image.php?id=103528&page=18, shows PHB>AVG adjacent processes, pseudo labeled in green (AVG) and red (PHB).

b: Print #359, JSE series (JSE_122257), http://wormimage.org/image.php?id=122257&page=2, and print #500, N2Y series (PAG500), http://wormimage.org/image.php?id=103408&page=20, shows AVG>VD13 adjacent processes, pseudo labeled in green (AVG) and pink (VD13).

c: Print #377, JSE series (JSE_122275), http://wormimage.org/image.php?id=122275&page=2, and print #800, N2Y series (PAG800), http://wormimage.org/image.php?id=103706&page=16, shows PHA>AVG adjacent processes, pseudo labeled in green (AVG) and orange (PHA).

d: A table summarizing the number of EM sections in which direct adjacency of processes was observed. Over a 1000 PAG (preanal ganglion) serial sections were analyzed for each sex.

a

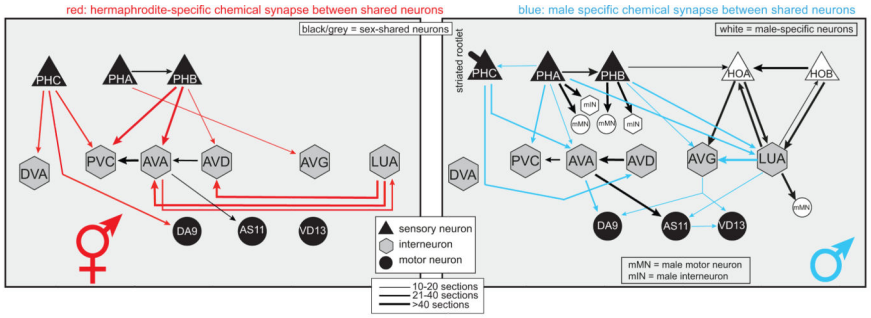

b

GRASP and/or iBLINC

Pre	Post	Sex	*Presynaptic marker*	*Postsynaptic marker*
LUA	AVG	♂	*eat-4p9::NLG-1::spGFP1-10* *eat-4p9::BirA::NRX-1*	*inx-18p::NLG-1::spGFP11* *inx-18p::AP::NLG-1*
	AVA	♀	*eat-4p9::NLG-1::spGFP1-10*	*flp-18p::NLG-1::spGFP11*

c

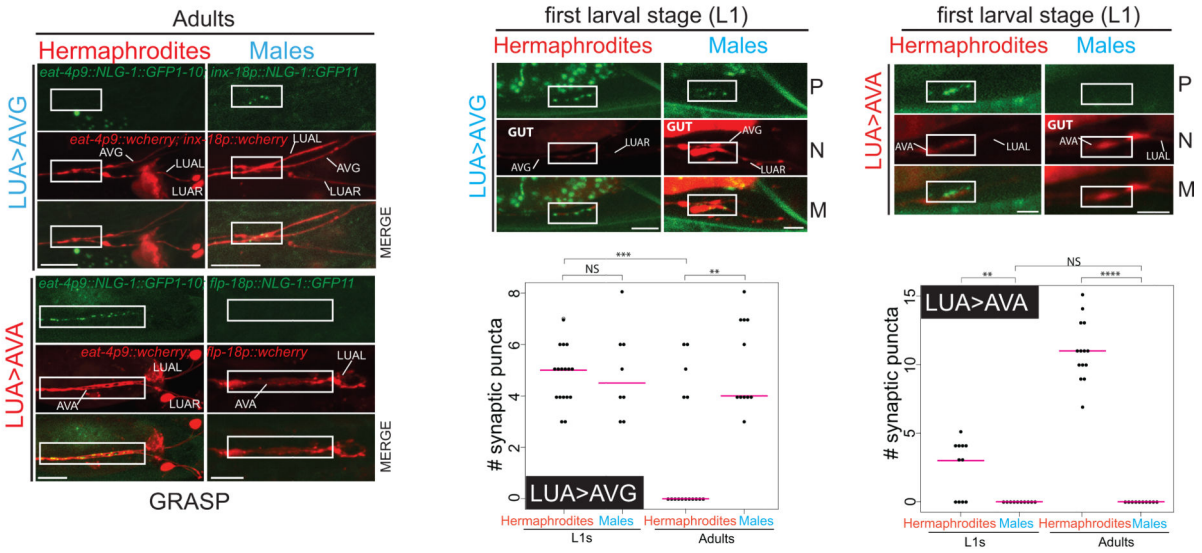

d

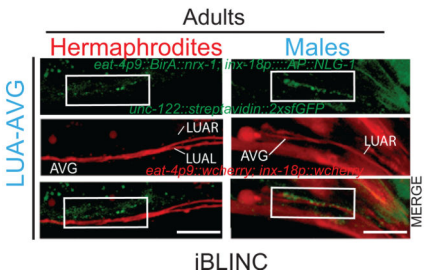

Extended Data Figure 2.

a: The connectivity diagram shown in Fig. 1a but now also including dimorphic connections of the LUA and PHC connections. The GRASP data that we show in this figure as well as the pruning data, sexual reversal data and mutant data shown in other Extended Figures, supports the original LUA connectivity data reported in Ref.3 and summarized in this schematic. However, a recent reassessment of the tracing of electron micrographs suggests that the connectivity assignments of the PHC and LUA neurons may have been swapped with each other (Scott Emmons, pers. comm.).

b: Overview of LUA synaptic connections labeled in this paper.

c: Visualizing LUA sexually dimorphic synapses. Quantification and fluorescent micrographs of GRASP transsynaptically labeled puncta between LUA>AVG and LUA>AVA, in L1 and adult hermaphrodites and males. The P, M and N letters next to fluorescent images denote labeling of **P**uncta, **N**eurite and **M**erge, respectively. Region of neurite overlap and observed synaptic puncta marked with white boxes. Gut; auto-fluorescence gut granules. Scale bars are 10μM for adult fluorescent panels and 5 μM for L1 panels.

d: Fluorescent micrographs of the preanal ganglion region of transgenic animals expressing the presynaptic BirA::nrx-1 fusion in LUA (using the *eat-4p9* promoter), and postsynaptic acceptor peptide::nlg-1 fusion in AVG. For more details see Extended data Figure 3. Scale bars are 10 μM

We performed the nonparametric Mann-Whitney test (Wilcoxon rank sum test) with Bonferroni correction for multiple comparisons. ****$P < 0.0001$, ***$P < 0.001$, **$P < 0.01$, NS; non significant. Magenta horizontal bars represent the median.

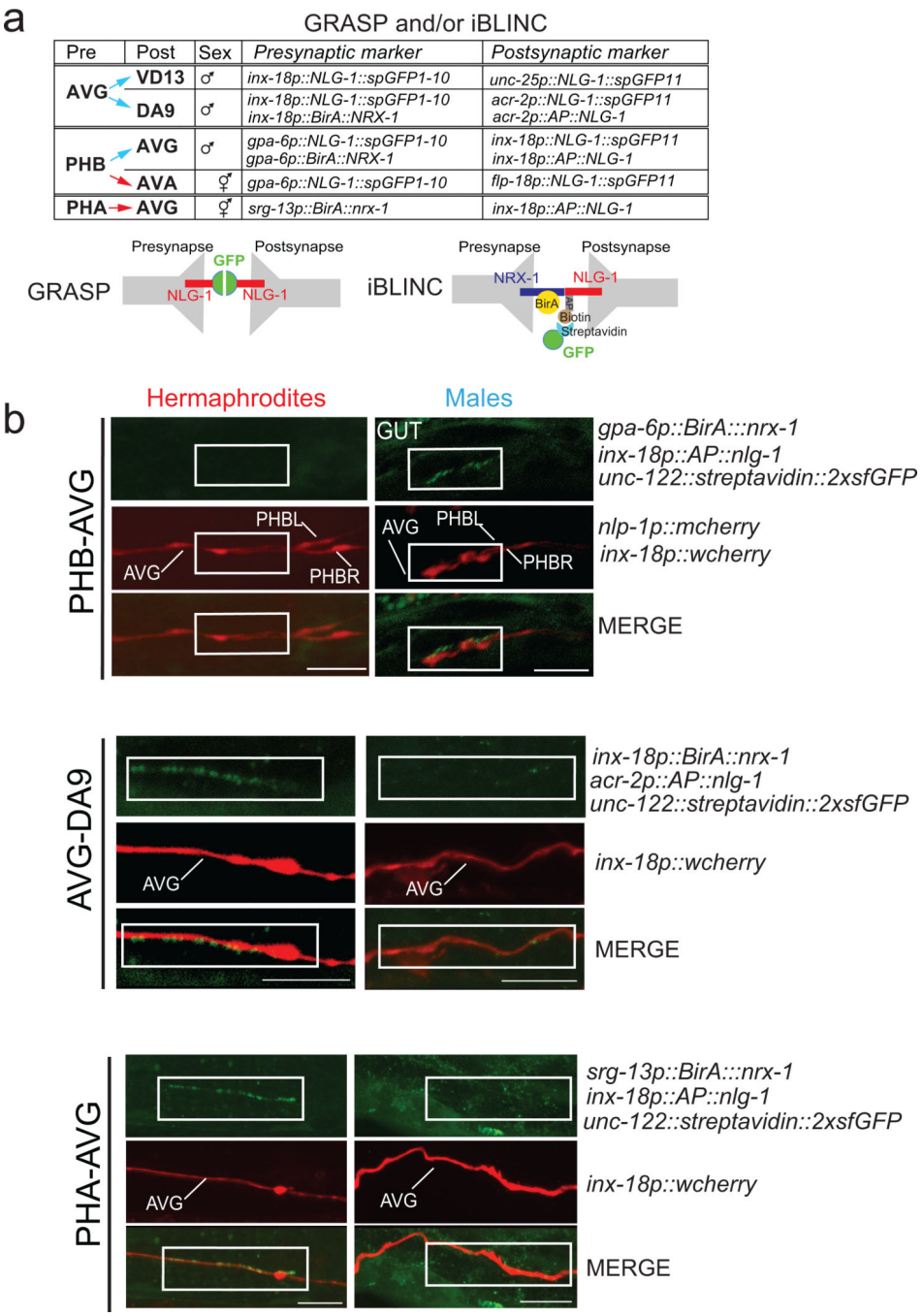

Extended Data Figure 3. Transsynaptic labeling of dimorphic connections using iBLINC

a: Overview of synaptic connections labeled in this paper (Fig. 1 and this figure). Some connections were labeled with both GRASP and iBLINC, yielding similar results. We generally note that the number of synapses is roughly reproducible from animal to animal and the number of the fluorescent dots is roughly comparable to the number of synapses identified by the EM analysis. However, there is also some variance from animal to animal (quantified in Fig. 3), consistent with previous analysis [40].

b: Labeling data not shown in Fig. 1. Fluorescent micrographs of the preanal ganglion region of transgenic animals expressing the presynaptic BirA::nrx-1 fusion in PHB (using the *gpa-6* promoter), AVG (using the *inx-18* promoter) and PHA (using the *srg-13* promoter), and postsynaptic acceptor peptide::nlg-1 fusion in AVG and DA9 (using the *acr-2* promoter). Transgenic worms also express the streptavidin detector fused to 2xsfGFP from the coelomocytes (*unc-122* promoter) [8]. Neuronal processes are labeled with cytoplasmic Cherry markers of the iBLINC pairs. Region of neurite overlap and observed synaptic puncta are marked with white boxes. Gut; auto-fluorescence gut granules. Scale bars are 10 μM. Anterior is left and dorsal is up.

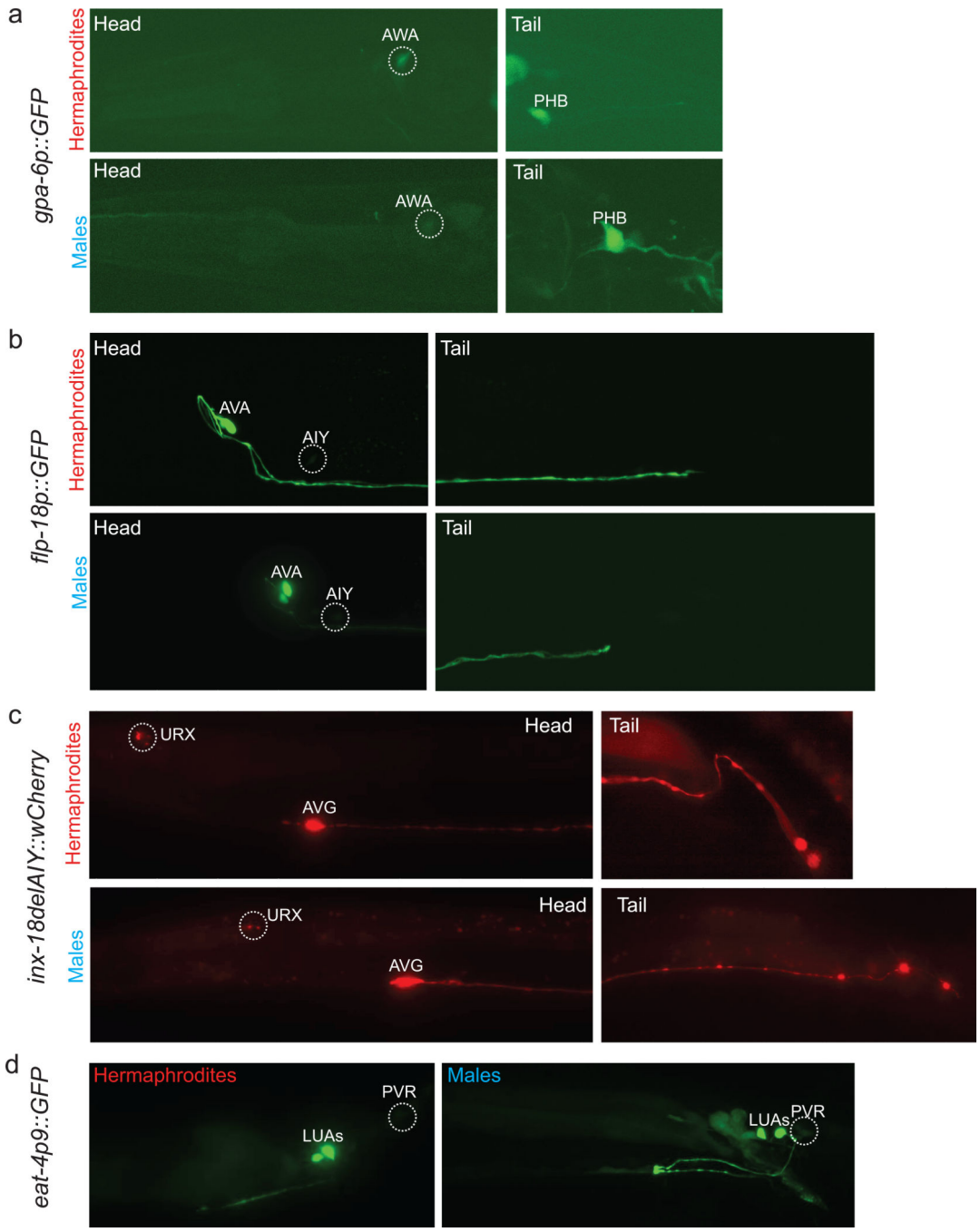

Extended Data Figure 4. Specificity of driver lines

a: A 2.6 kb *gpa-6* promoter fragment fused to GFP is expressed consistently in PHB at all stages. There is also faint and variable expression in AWA.

b: The 3.1kb *flp-18* promoter fused to GFP is expressed consistently in AVA, and dimly and variably in AIY (85% of animals) and RIM (15% of animals), which were identified based on comparison to published *flp-18* expression patterns [41].

c: The 1.8 kb *inx-18* 2nd intron fused to codon optimized Cherry is expressed brightly and consistently in AVG, and dimly and variably in URXs. The AIY motif present in this fragment was deleted (see Methods).

d: The 170 bp *eat-4* promoter (eat-4p9) fused to GFP is expressed in LUAs and PVR.

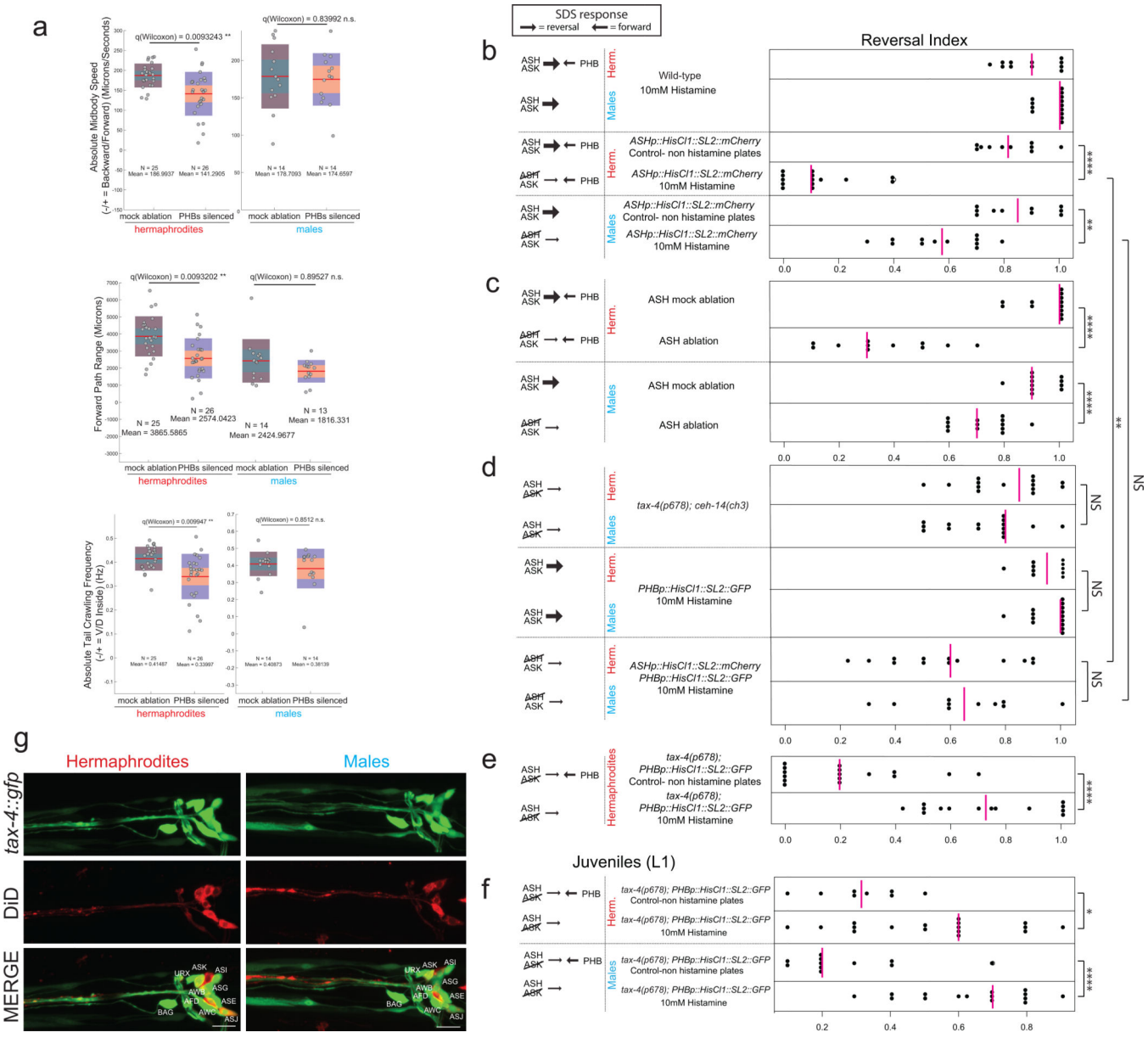

Extended Data Figure 5. Additional SDS avoidance assays

a: PHB silenced hermaphrodites move slower forward (quantified as absolute midbody speed) and as a result cover less of the plate (quantified as forward path range) compared with control hermaphrodites, while PHB silenced males do not show any difference from control males. In addition, the tail-bending wave is affected in PHB silenced hermaphrodites, but not in males (quantified as tail crawling frequency). Statistics were computed using Wilcoxon rank-sum, and correction for multiple testing (q-values) was

computed across all measures (roughly 1404 tests) using the Benjamini–Hochberg procedure.

b: Silencing of ASH neuronal activity using the histamine chloride channel 1(HisCl1) affects the animals' chemosensory avoidance response.

Males and hermaphrodites were assayed for affects of histamine on SDS avoidance behavior. We used the *him-5* mutant background (which gives a high incidence of male progeny) as wild type. There is no difference between worms assayed in the presence and absence of histamine (Fig. 2a). The avoidance index of single animals was calculated as the fraction of reversal responses in 10 or more assays, depicted as black dots. Magenta vertical bars represent the median.

L4 animals carrying the *kyEx5104 [pNP424 (sra-6::HisCl1::SL2::mCherry)]*[β] transgene were grown on 10mM histamine-containing NGM plates for 24 hours. As a control, *kyEx5104* animals were grown on NGM plates without histamine. ASH silencing reduces the head sensory response to SDS, thus in hermaphrodites the antagonizing activity of the PHBs inhibits the backward movement and the worms do not reverse. In males, no such antagonizing activity occurs and the worms reverse, albeit with reduced ability.

c: Ablation of ASH neurons affects the animals' chemosensory avoidance response in a similar manner to histamine-induced silencing. *sra-6::gfp* was used to identify the ASH neurons.

d: Behavioral differences stem from dimorphic connectivity differences and not from amphid/ phasmid sensory function. *tax-4; ceh-14* double mutants behave in a similar manner in both sexes. PHB silencing (*gpa-6::HisCl1::SL2::GFP*) doesn't affect the worms behavior in both sexes. Silencing both the ASHs and PHBs in males showed no difference from ASH silenced males, but silencing ASHs and PHBs in hermaphrodites showed a significant difference from ASH silenced hermaphrodites, where we expect the PHBs to function in an antagonistic manner, and thus in its absence, ASH silenced hermaphrodites now show an increase in their ability to respond to SDS by reversing.

e: PHB silencing in *tax-4* mutant background. *tax-4* is a subunit of a cyclic nucleotide gated channel expressed in chemosensory and thermosensory neurons [42], see panel **g**, *tax-4* animals show a strongly reduced avoidance response to SDS [10]. Silencing of PHBs in *tax-4* hermaphrodies eliminated the antagonizing affect and animals are able to avoide SDS by backing.

f: PHB silencing in *tax-4* mutant background at the L1 stage. Lack of avoidance seen in *tax-4* L1 males and hermaphrodites depends on PHB function.

For all panels, we performed the nonparametric Mann-Whitney test with Bonferroni correction for multiple comparisons. **** $P < 0.0001$, ** $P < 0.01$, * $P < 0.05$, NS; non significant.

g:*tax-4* expression pattern is identical in hermaphrodites and males. *kyEx744 (tax-4p::TAX-4::GFP)*[42], was analyzed in adult male and hermaphrodites. Amphid neurons in the head (ADL, ASH, ASI, ASJ, ASK, AWB) were stained using DiD to facilitate cell identification. Neurons identified, shown in "Merge" panel are identical in both sexes and match published data. All neurons are bilaterally symmetric left-right pairs, and for simplicity only left cells are shown. Scale bars are 10 μM.

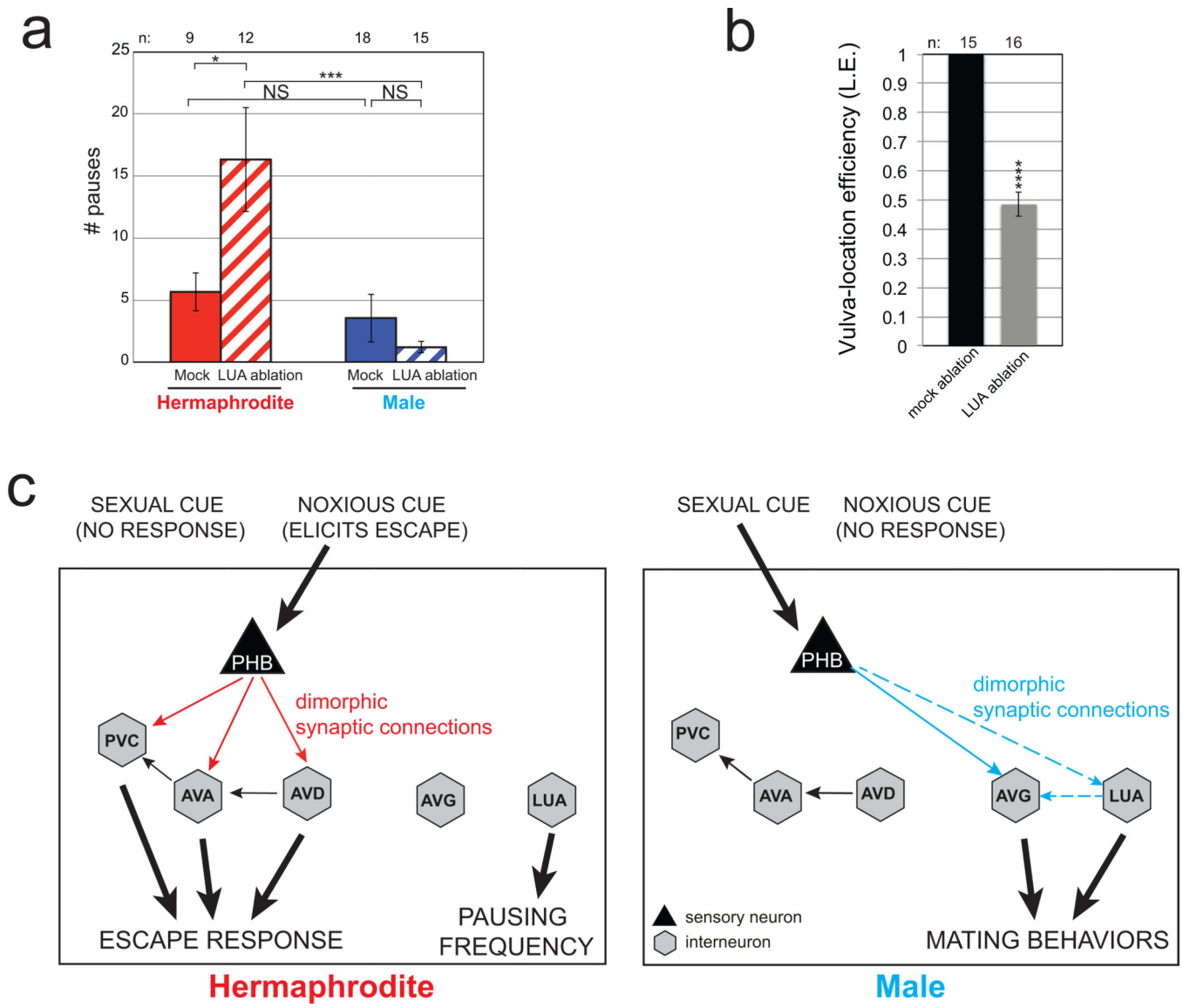

Extended Data Figure 6. Additional behavioral analysis

a: Hermaphrodites in which LUAs have been ablated pause more frequently than mock-ablated hermaphrodites and LUA-ablated males. Error bars are S.E.M.

b: LUA laser-ablated animals tested for the male's vulva location efficiency. The behavioral data shown in panel a and b supports the reported connectivity data shown in Extended Figure 2.

In panels **a, b** we performed the nonparametric Mann-Whitney test (Wilcoxon rank sum test) with Bonferroni correction for multiple comparisons. Error bars in **b** are S.E.M. $***P < 0.001$, $*P < 0.05$, NS; non significant.

c: Summary of dimorphic behaviors induced by PHB sensory neurons and AVG/LUA interneurons.

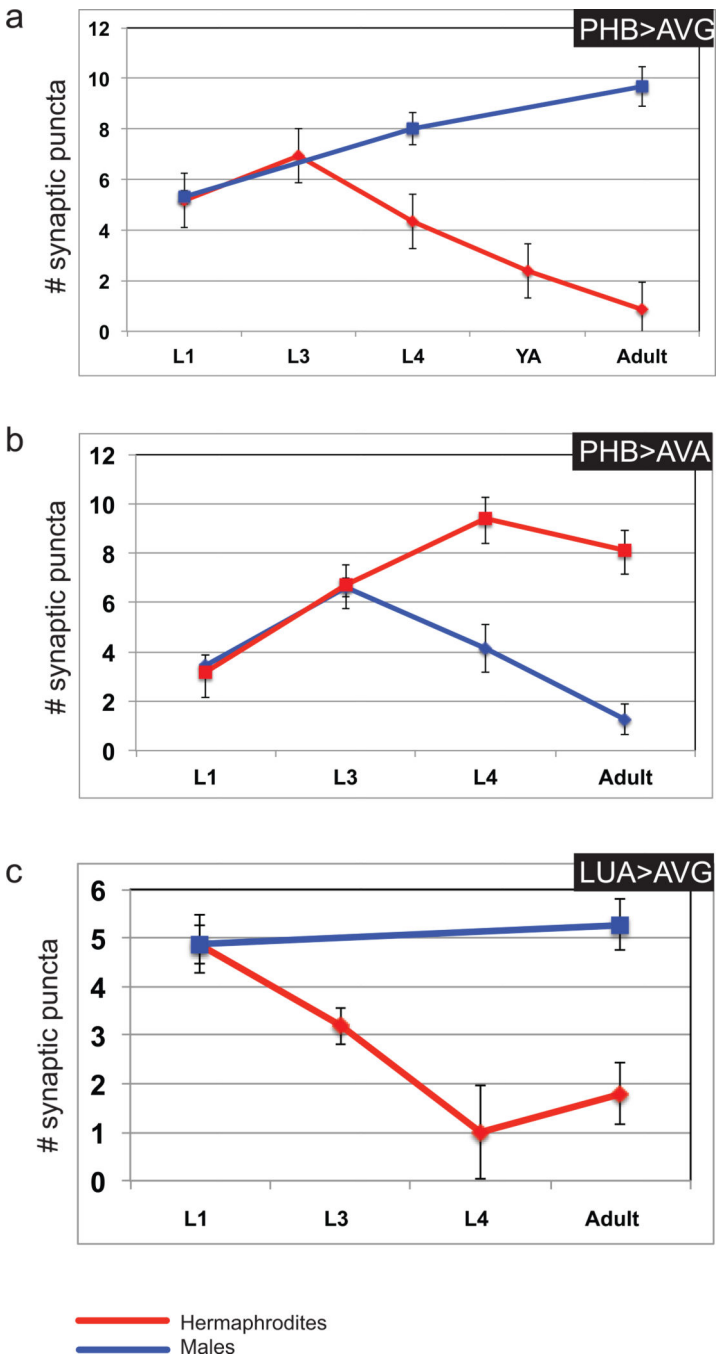

Extended Data Figure 7. Time course analysis of synapse pruning and development

Hermaphrodites and males were analyzed at the L1, L3, L4, young adult and gravid adult stages, and the number of synaptic puncta observed at each stage was plotted against developmental time points. Synaptic puncta in hermaphrodites are plotted in red, synaptic puncta in males are plotted in blue.

a: PHB>AVG synapses are pruned in hermaphrodites at the L3 stage.

b: PHB>AVA synapses are pruned in males at the L3 stage.

c: LUA>AVG synapses are pruned earlier, starting at the L1 stage in hermaphrodites.

Error bars are SEM, and for each time point depicted in graphs, at least 15 animals were analyzed.

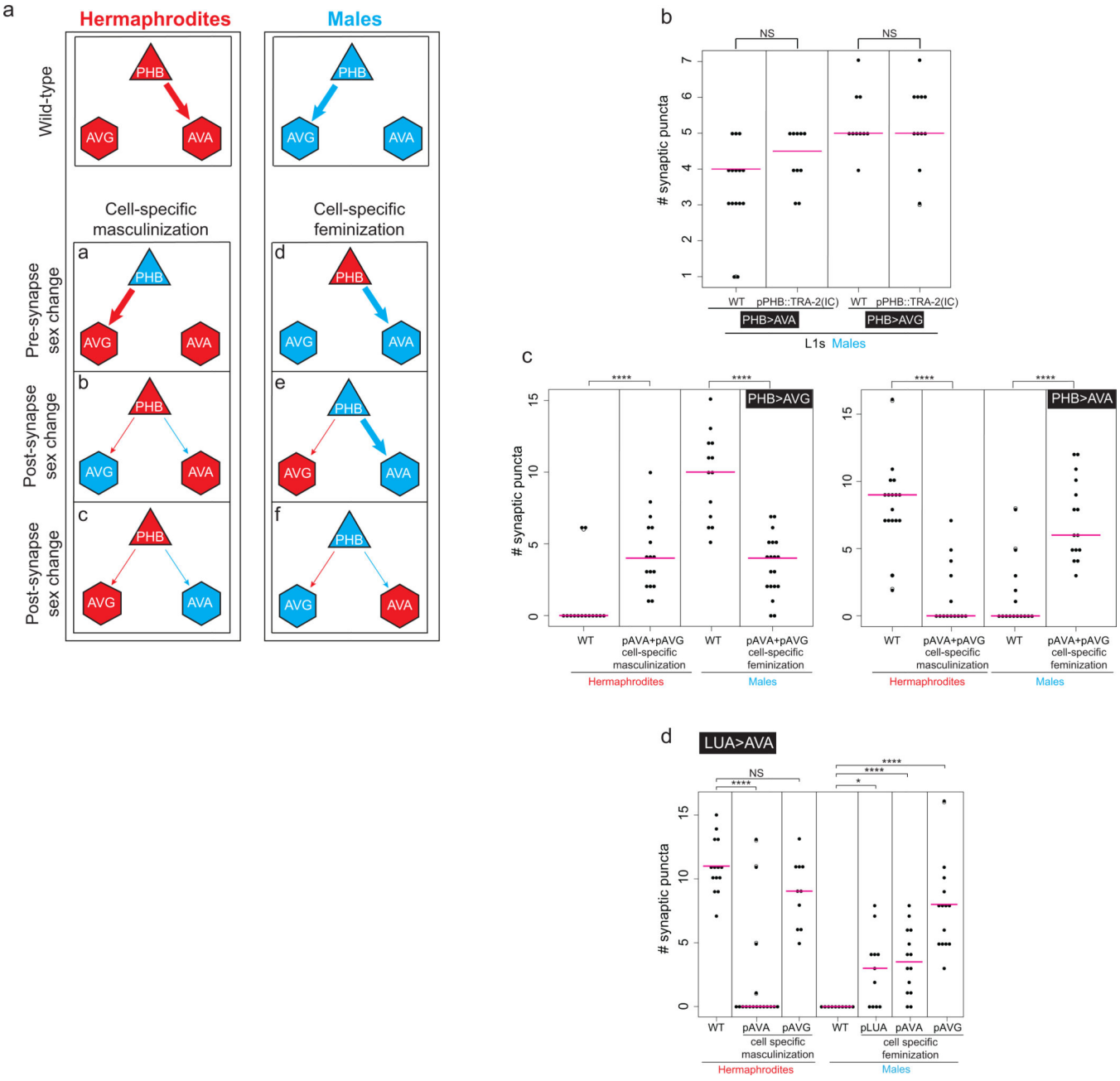

Extended Data Figure 8. Autonomy and non-autonomy of sex-specific synapse pruning

a: Cartoon summarizing sex changes effects on synapses.

b: L1-stage connectivity is not affected by sex-reversal.

c: Simultaneous sex reversal of both AVA and AVG.

d: Sex reversal experiments. Masculinization of the postsynaptic cell AVA is sufficient to induce LUA>AVA synaptic puncta in hermaphrodites. The postsynaptic cell AVA was masculinized by expression of FEM-3 and the number of synaptic puncta was measured.

Masculinization of AVG was not sufficient to induce synapses between LUA and AVA in hermaphrodites. Feminizing LUA, AVA and AVG by expression of TRA-2^{IC} was sufficient to induce ectopic LUA>AVA puncta in males.

We performed the nonparametric Mann-Whitney test with Bonferroni correction for multiple comparisons. ****$P < 0.0001$, ****$P < 0.01$, NS*; Not significant*. Magenta horizontal bars represent the median.

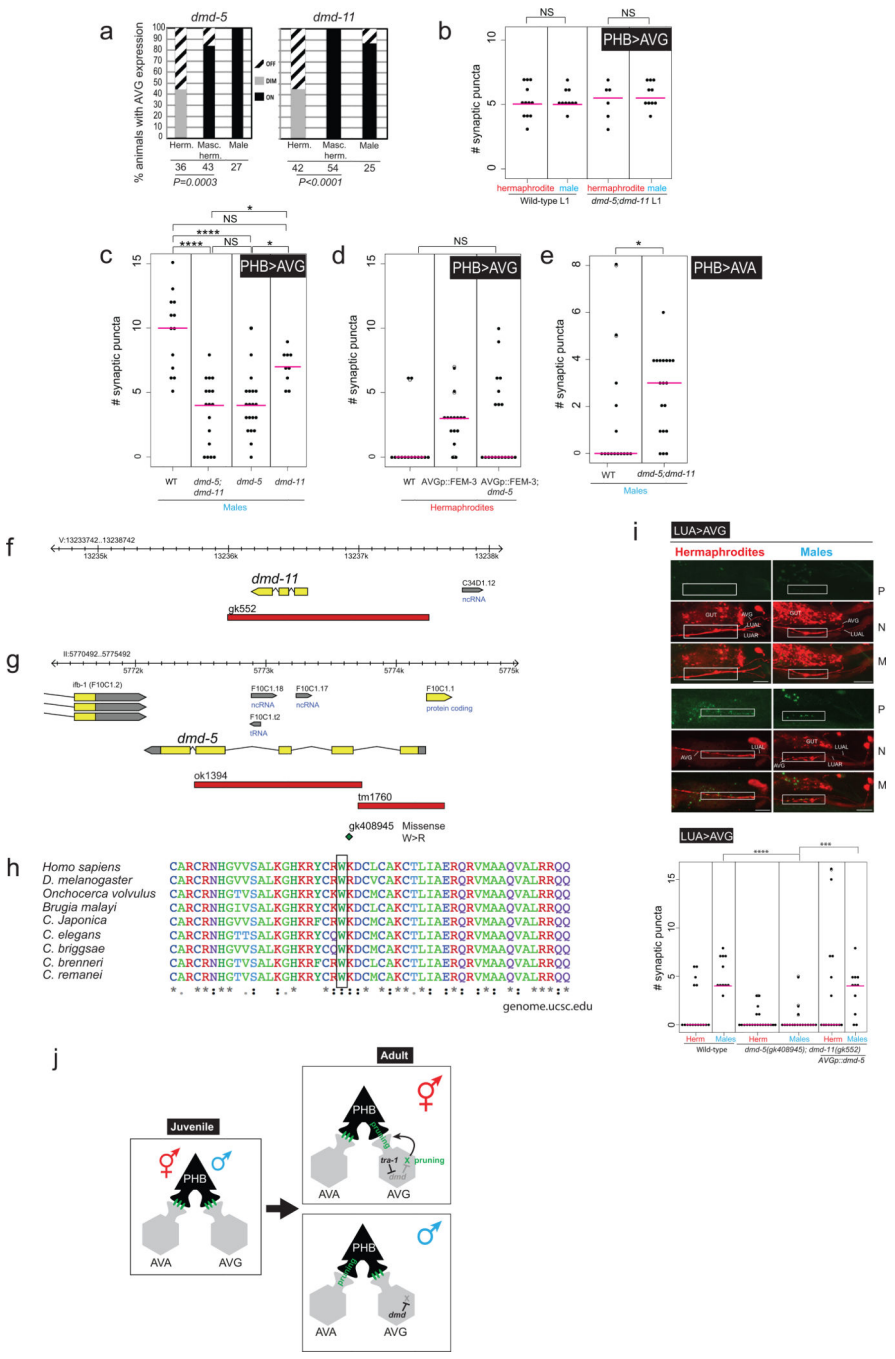

Extended Data Figure 9. *dmd-5* and *dmd-11* expression, sequence and function

a: Quantification of dimorphic expression of *dmd-5* and *dmd-11* in AVG. Expression in hermaphrodites was off or extremely faint. Expression of *inx-18p::FEM-3* derepressed *dmd-5* and *dmd-11* gene expression in hermaphrodite AVGs. Statistics calculated using Fischer's Exact test.

b: Quantification of the number of PHB-AVG synaptic puncta in L1 *dmd-5(gk408945); dmd-11(gk552)* double mutants, compared with wild-type L1 animals. At the L1 stage *dmd-5* and *dmd-11* do not affect PHB-AVG synapses, suggesting they are required for maintenance of mature synapses.

c:*dmd-5* single mutants and *dmd-5; dmd-11* double mutants display similar alterations in AVG synaptic wiring.

d:*dmd-5* mutation suppresses the ectopic PHB>AVG synapses in AVG-masculinized animals.

e: The PHB>AVA connection is non-autonomously partially stabilized in *dmd-5; −11* mutants.

f:*dmd-11* genomic locus and *gk552* deletion location.

g:*dmd-5* genomic locus and mutation description. *ok1394* location was not curated, to determine location we used the following primers: Forward primer: cagaatgcctgtttctccgtc and Reverse: cactgcttttcccgttcaaac. *ok1394* and *tm1760* were both found to have an embryonic lethal phenotype that couldn't be rescued with the genomic locus (data not shown), thus we searched for single point mutations of the "million mutation project"[43] *gk408945* is a missense substitution mutation of W54 to R, located in the second exon. Genomic analysis revealed that this mutation lies within the conserved DM domain (**e**.), with perfect conservation across evolution. The DM domain is an intertwined zinc-containing DNA binding module. The DM domain binds DNA as a dimer, allowing the recognition of pseudopalindromic sequences [44].

h: DM-domain sequence conservation and location of *gk408945* mutation. Conservation and multiple sequence alignment were done using UCSC Genome Browser (genome.ucsc.edu) and ClustalW.

i:*dmd-5* and *dmd-11* are required for maintenance of AVG synapses. Fluorescent micrographs and quantification of synaptic puncta of LUA>AVG. Region of neurite overlap and observed synaptic puncta marked with white boxes. The P, M and N letters next to fluorescent images denote labeling of **P**uncta, **N**eurite and **M**erge, respectively.

In b, d , e and **i** statistics were calculated using the nonparametric Mann-Whitney test. In panel c statistics were calculated using Kruskal-Wallis test with Dunn's multiple comparison test. ****$P < 0.0001$, ***$P < 0.001$, *$P < 0.05$, NS*; Not significant*. Magenta horizontal bars represent the median. When using a parametric t-test, there is also a significant difference for the LUA>AVG synapse between *dmd-5;dmd-11* mutant hermaphrodites and *dmd-5;dmd-11* mutant hermaphrodites that over express DMD-5 (*$P < 0.05$).

j: Summary of data. TRA-1 and DMD proteins are commonly thought to work as transcriptional repressors [22]. Since *dmd-5/11* are already dimorphically expressed in AVG in embryos and L1 stage animals (not shown in this schematic), there must be other timer mechanisms that control the onset of pruning. For example, DMD-5/11 may work together with a regulatory factor of the stage-specifically acting heterochronic pathway. Furthermore, we hypothesize that other neurons, such as the AVA neuron, may have its own complement of sex-specific *dmd* genes that control pruning.

Supplementary Material

Refer to Web version on PubMed Central for supplementary material.

Acknowledgments

We thank Qi Chen for generating transgenic strains, John White, John Sulston and LMB/MRC for sharing their annotated EM images to David Hall for curation, and www.wormimage.org where these annotated images have been made available by David Hall, Eviatar Yemini for advice on tracking experiments, Steven Cook for help with Elegance software, Mei Zhen for communicating unpublished results, Piali Sengupta, Iva Greenwald and member of the Hobert lab for comments on the manuscript. This work was supported by postdoctoral fellowships from the EMBO and HFSP (to M.O.), the NIH (2R37NS039996) and the HHMI. Meital Oren-Suissa is an Awardee of the Weizmann Institute of Science – National Postdoctoral Award Program for Advancing Women in Science.

REFERENCES

1. Sulston JE, Schierenberg E, White JG, Thomson JN. The embryonic cell lineage of the nematode Caenorhabditis elegans. Dev Biol. 1983; 100:64–119. [PubMed: 6684600]
2. Sammut M, et al. Glia-derived neurons are required for sex-specific learning in C. elegans. Nature. 2015; 526:385–390. [PubMed: 26469050]
3. Jarrell TA, et al. The connectome of a decision-making neural network. Science. 2012; 337:437–444. [PubMed: 22837521]
4. Emmons SW. The development of sexual dimorphism: studies of the Caenorhabditis elegans male. Wiley Interdiscip Rev Dev Biol. 2014; 3:239–262. [PubMed: 25262817]
5. Portman DS. Genetic control of sex differences in C. elegans neurobiology and behavior. Adv Genet. 2007; 59:1–37. [PubMed: 17888793]
6. White JG, Southgate E, Thomson JN, Brenner S. The structure of the nervous system of the nematode *Caenorhabditis elegans* Philosophical Transactions of the Royal Society of London B. Biological Sciences. 1986; 314:1–340. [PubMed: 22462104]
7. Feinberg EH, et al. GFP Reconstitution Across Synaptic Partners (GRASP) defines cell contacts and synapses in living nervous systems. Neuron. 2008; 57:353–363. [PubMed: 18255029]
8. Desbois M, Cook SJ, Emmons SW, Bulow HE. Directional Trans-Synaptic Labeling of Specific Neuronal Connections in Live Animals. Genetics. 2015
9. Pokala N, Liu Q, Gordus A, Bargmann CI. Inducible and titratable silencing of Caenorhabditis elegans neurons in vivo with histamine-gated chloride channels. Proc Natl Acad Sci U S A. 2014; 111:2770–2775. [PubMed: 24550306]
10. Hilliard MA, Bargmann CI, Bazzicalupo PC. elegans responds to chemical repellents by integrating sensory inputs from the head and the tail. Curr Biol. 2002; 12:730–734. [PubMed: 12007416]
11. Serrano-Saiz E, et al. Modular Control of Glutamatergic Neuronal Identity in C. elegans by Distinct Homeodomain Proteins. Cell. 2013; 155:659–673. [PubMed: 24243022]
12. Liu KS, Sternberg PW. Sensory regulation of male mating behavior in Caenorhabditis elegans. Neuron. 1995; 14:79–89. [PubMed: 7826644]
13. Sherlekar AL, The C, et al. elegans male exercises directional control during mating through cholinergic regulation of sex-shared command interneurons. PLoS One. 2013; 8:e60597. [PubMed: 23577128]
14. Yemini E, Jucikas T, Grundy LJ, Brown AE, Schafer WR. A database of Caenorhabditis elegans behavioral phenotypes. Nat Methods. 2013; 10:877–879. [PubMed: 23852451]
15. Sulston JE, Horvitz HR. Post-embryonic cell lineages of the nematode, Caenorhabditis elegans. Dev Biol. 1977; 56:110–156. [PubMed: 838129]
16. Sulston JE, Albertson DG, Thomson JN. The Caenorhabditis elegans male: postembryonic development of nongonadal structures. Dev Biol. 1980; 78:542–576. [PubMed: 7409314]
17. Mowrey WR, Bennett JR, Portman DS. Distributed effects of biological sex define sex-typical motor behavior in Caenorhabditis elegans. J Neurosci. 2014; 34:1579–1591. [PubMed: 24478342]

18. White JQ, et al. The sensory circuitry for sexual attraction in C. elegans males. Curr Biol. 2007; 17:1847–1857. [PubMed: 17964166]
19. Lee K, Portman DS. Neural sex modifies the function of a C. elegans sensory circuit. Curr Biol. 2007; 17:1858–1863. [PubMed: 17964163]
20. Mehra A, Gaudet J, Heck L, Kuwabara PE, Spence AM. Negative regulation of male development in Caenorhabditis elegans by a protein-protein interaction between TRA-2A and FEM-3. Genes Dev. 1999; 13:1453–1463. [PubMed: 10364161]
21. Yang CF, Shah NM. Representing sex in the brain, one module at a time. Neuron. 2014; 82:261–278. [PubMed: 24742456]
22. Matson CK, Zarkower D. Sex and the singular DM domain: insights into sexual regulation, evolution and plasticity. Nat Rev Genet. 2012; 13:163–174. [PubMed: 22310892]
23. Hutter H. Extracellular cues pioneers act together to guide axons in the ventral cord of C. elegans. Development. 2003; 130:5307–5318. [PubMed: 13129845]

References for Methods

24. Brenner S. The genetics of Caenorhabditis elegans. Genetics. 1974; 77:71–94. [PubMed: 4366476]
25. Wenick AS, Hobert O. Genomic cis-Regulatory Architecture trans-Acting Regulators of a Single Interneuron-Specific Gene Battery in C. elegans. Dev Cell. 2004; 6:757–770. [PubMed: 15177025]
26. Hobert O. PCR fusion-based approach to create reporter gene constructs for expression analysis in transgenic C. elegans. Biotechniques. 2002; 32:728–730. [PubMed: 11962590]
27. Bond SR, Naus CC. RF-Cloning.org: an online tool for the design of restriction-free cloning projects. Nucleic Acids Res. 2012; 40:W209–W213. [PubMed: 22570410]
28. Jansen G, et al. The complete family of genes encoding G proteins of Caenorhabditis elegans. Nat Genet. 1999; 21:414–419. [PubMed: 10192394]
29. Park J, et al. A conserved juxtacrine signal regulates synaptic partner recognition in Caenorhabditis elegans. Neural Dev. 2011; 6:28. [PubMed: 21663630]
30. Nathoo AN, Moeller RA, Westlund BA, Hart AC. Identification of neuropeptide-like protein gene families in Caenorhabditiselegans and other species. Proc Natl Acad Sci U S A. 2001; 98:14000–14005. [PubMed: 11717458]
31. Eastman C, Horvitz HR, Jin Y. Coordinated transcriptional regulation of the unc-25 glutamic acid decarboxylase and the unc-47 GABA vesicular transporter by the Caenorhabditis elegans UNC-30 homeodomain protein. J Neurosci. 1999; 19:6225–6234. [PubMed: 10414952]
32. Jospin M, et al. A neuronal acetylcholine receptor regulates the balance of muscle excitation and inhibition in Caenorhabditis elegans. PLoS Biol. 2009; 7:e1000265. [PubMed: 20027209]
33. Troemel ER, Chou JH, Dwyer ND, Colbert HA, Bargmann CI. Divergent seven transmembrane receptors are candidate chemosensory receptors in C. elegans. Cell. 1995; 83:207–218. [PubMed: 7585938]
34. Fang-Yen C, Gabel CV, Samuel AD, Bargmann CI, Avery L. Laser microsurgery in Caenorhabditis elegans. Methods Cell Biol. 2012; 107:177–206. [PubMed: 22226524]
35. Garcia LR, LeBoeuf B, Koo P. Diversity in mating behavior of hermaphroditic and male-female Caenorhabditis nematodes. Genetics. 2007; 175:1761–1771. [PubMed: 17277358]
36. Peden EM, Barr MM. The KLP-6 kinesin is required for male mating behaviors and polycystin localization in Caenorhabditis elegans. Curr Biol. 2005; 15:394–404. [PubMed: 15753033]
37. Gordus A, Pokala N, Levy S, Flavell SW, Bargmann CI. Feedback from network states generates variability in a probabilistic olfactory circuit. Cell. 2015; 161:215–227. [PubMed: 25772698]
38. Xu M, et al. Computer Assisted Assembly of Connectomes from Electron Micrographs: Application to Caenorhabditis elegans. PLoS ONE. 2013; 8:e54050. [PubMed: 23342070]
39. White, jG. Neuronal connectivity in Caenorhabditis elegans. Trends Neurosci. 1985; 8:277–283.
40. Durbin, RM. Ph.D. thesis. University of Cambridge; 1987.
41. Rogers C, et al. Inhibition of Caenorhabditis elegans social feeding by FMRFamide-related peptide activation of NPR-1. Nat Neurosci. 2003; 6:1178–1785. [PubMed: 14555955]

42. Komatsu H, Mori I, Rhee JS, Akaike N, Ohshima Y. Mutations in a cyclic nucleotide-gated channel lead to abnormal thermosensation and chemosensation in C. elegans. Neuron. 1996; 17:707–718. [PubMed: 8893027]

43. Thompson O, et al. The million mutation project: a new approach to genetics in Caenorhabditis elegans. Genome Res. 2013; 23:1749–1762. [PubMed: 23800452]

44. Murphy MW, et al. An ancient protein-DNA interaction underlying metazoan sex determination. Nat Struct Mol Biol. 2015; 22:442–451. [PubMed: 26005864]

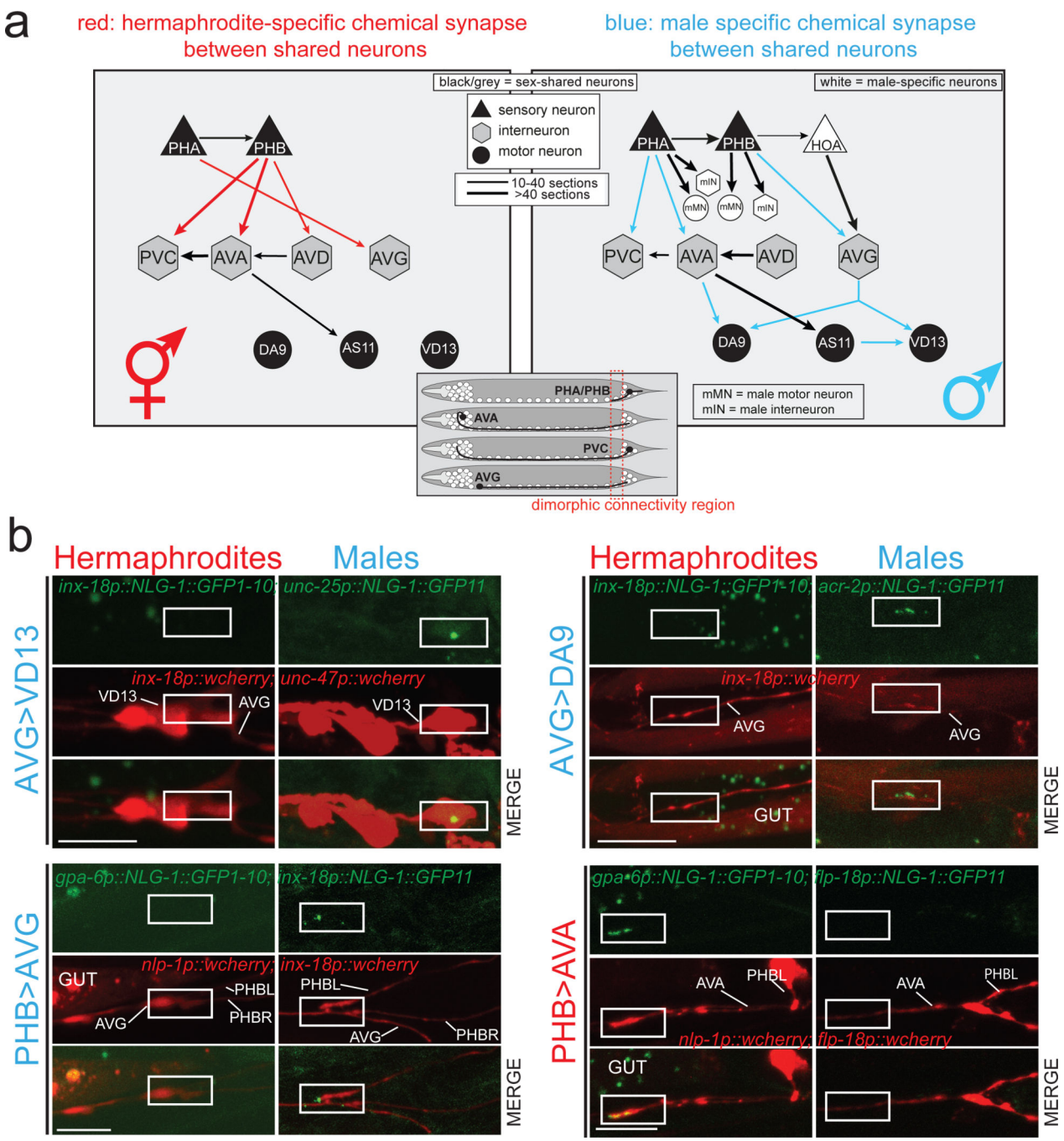

Figure 1. Visualizing sexually dimorphic synapses

a: Connectivity of selected neurons at the adult stage, as inferred from serial section reconstructions of electron micrographs[3]. Chemical synapses between sensory (triangles), inter- (hexagons) and motor (circles) neurons are depicted as arrows. Thickness of arrows correlates with degree of connectivity (number of sections over which en passant synapses are observed). The inset indicates where synaptic connections are formed.

b: Visualizing sexually dimorphic synapses. Fluorescent micrographs of GRASP GFP signal in preanal ganglion region outlined in the inset in Fig. 1a. Neuronal processes are labeled

with cytoplasmic codon optimized Cherry markers of the GRASP pairs. GRASP data is shown in this Figure, additional iBLINC data is shown in Extended Data Fig. 3. Expression pattern of the promoters used in this study to drive cell specific expression can be found in Extended Data Fig. 4. Quantification of data is shown in Fig. 3b; the number of fluorescent puncta (outlined with white boxes) is similar to those observed in the EM analysis[3]. Gut; auto-fluorescence gut granules. Scale bars are 10 μM. In all images anterior is left, and dorsal is up. Blue and red color-coding is used in all figures to distinguish male from hermaphrodite, respectively.

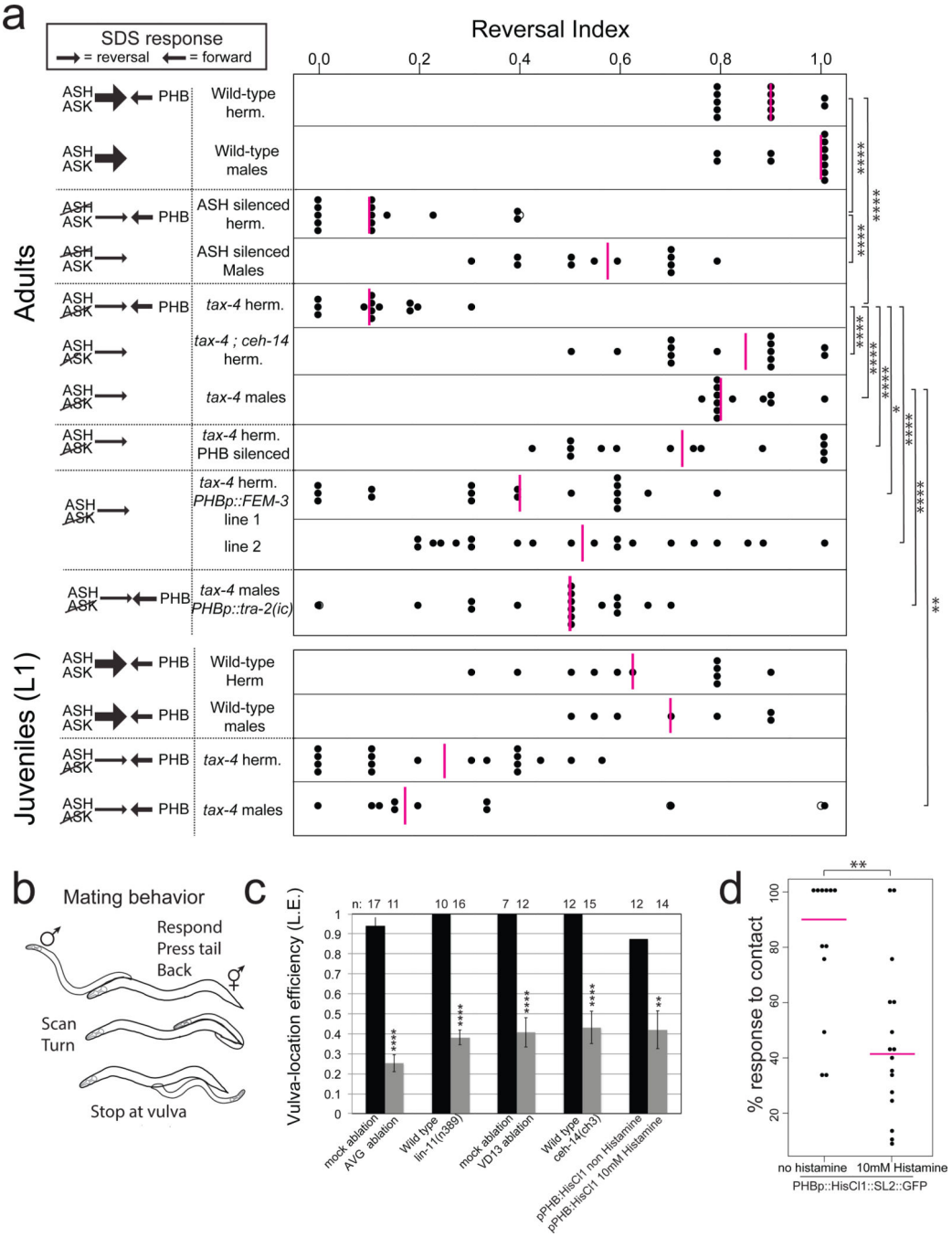

Figure 2. Functional repurposing of dimorphic neurons

a: Chemosensory repulsion assays (see Methods for full description of behavioral assays). Scatter diagrams plotting the avoidance index of single animals. Each black dot represents the fraction of reversal responses (scored as reversing or not reversing) in 10 or more assays of a single animal. Magenta vertical bars represent the median. The left column indicates predictions of reversal behavior, based on previously published data that demonstrated a strong reversal drive from head neurons (thick arrows) that is counteracted by a forward drive mediated by the PHB neurons in the tail[10]. Control experiments for silencing using

histamine and additional SDS assays can be found in Extended Data Fig. 5 *sra-6::HisCl1* and *gpa-6::HisCl1* were used for ASH and PHB silencing, respectively. Summary of dimorphic behaviors induced by PHB sensory neurons can be found in Extended Data Fig. 6c.

b: Changes in male movement and posture triggered by mate-contact[12].

c: Mutant or laser-operated animals tested for the male's vulva location efficiency. In *lin-11* and *ceh-14* mutants, the AVG and phasmid neurons, respectively, fail to differentiate[11,23]_ENREF_11.

d: Initiation of backward movement in response to hermaphrodite contact is dependent on PHB activity, measured as contact response efficiency. Each dot represents one animal.

In panels **a and c** we performed the nonparametric Mann-Whitney test (Wilcoxon rank sum test) with Bonferroni correction for multiple comparisons. Error bars in **c** are S.E.M. In panel **d** we performed Fisher's exact test. ****$P < 0.0001$, ***$P < 0.001$, **$P < 0.01$, *$P < 0.05$, NS; non significant in all panels.

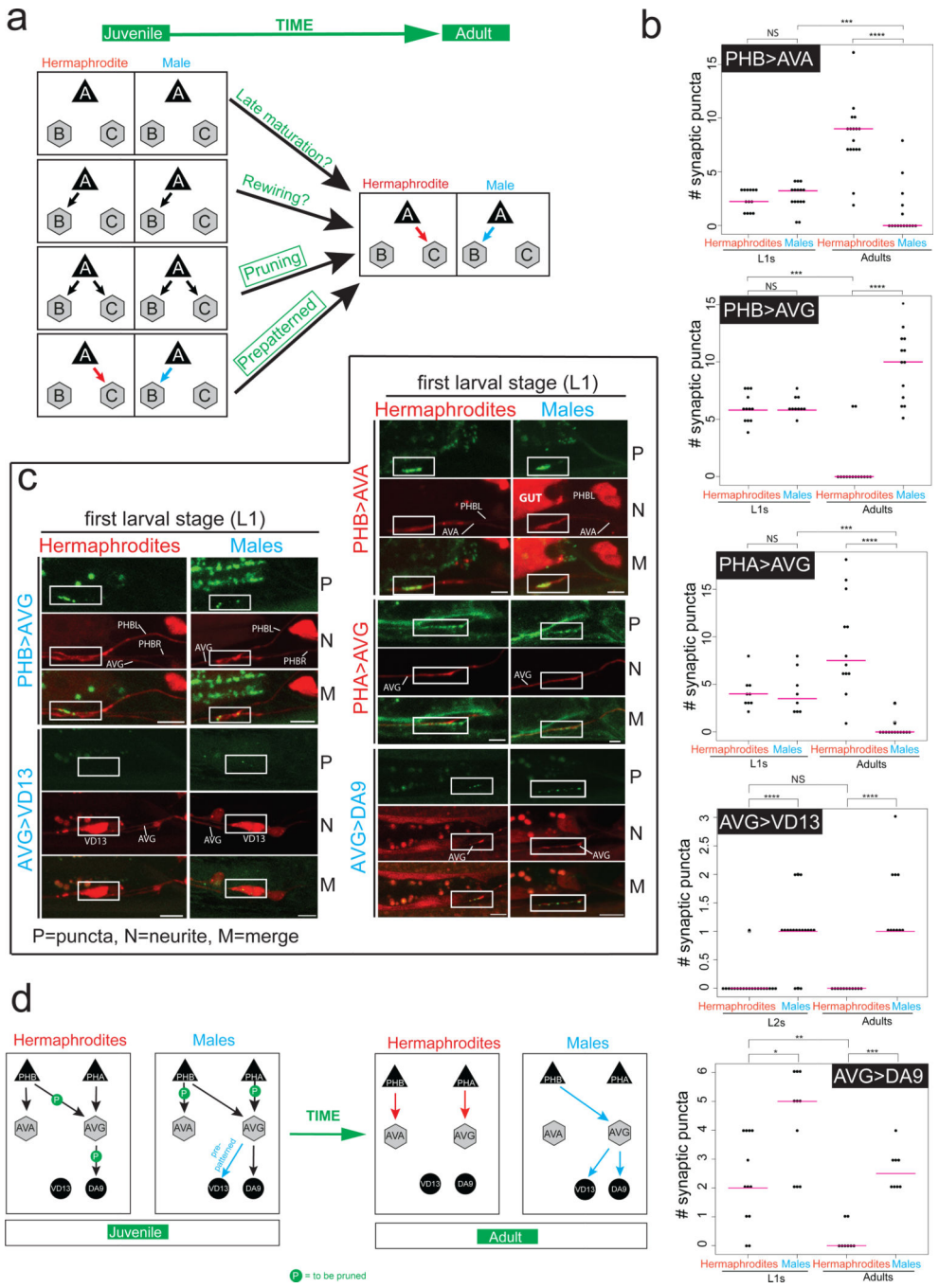

Figure 3. Synaptic pruning during development

a: Models for how sexually dimorphic connectivity patterns may arise during development.

b–c: Quantification and fluorescent micrographs of synaptic pruning measured by the number of synaptic puncta observed using GRASP GFP (PHB>AVA, PHB>AVG, AVG>VD13, AVG>DA9) and iBLINC GFP (PHA>AVG) in L1 and adult hermaphrodites and males. Since VD neurons are born at the end of the L1 stage, Juvenile VD13 puncta were quantified at the L2 stage.

We performed the nonparametric Mann-Whitney test (Wilcoxon rank sum test) with Bonferroni correction for multiple comparisons. **** $P < 0.0001$, *** $P < 0.001$, ** $P < 0.01$, * $P < 0.05$, NS; non significant. Magenta horizontal bars represent the median. The P, M and N letters next to fluorescent images denote labeling of **P**uncta, **N**eurite and **M**erge, respectively. Region of neurite overlap and observed synaptic puncta marked with white boxes. Gut; auto-fluorescence gut granules. Scale bars are 5 μM. Note that the roughly two-fold increase in synapse number from L1 to L4 in the hermaphroditic PHB>AVA connection and the male PHB>AVG is in line with an overall increase in total synapse numbers seen between neurons between L1 and adult stage as deduced by recent reconstruction of an L1 stage animal (M. Zhen, pers. comm.).

d: Summary of synaptic connection differences between juvenile, pre-L4 animals and adults.

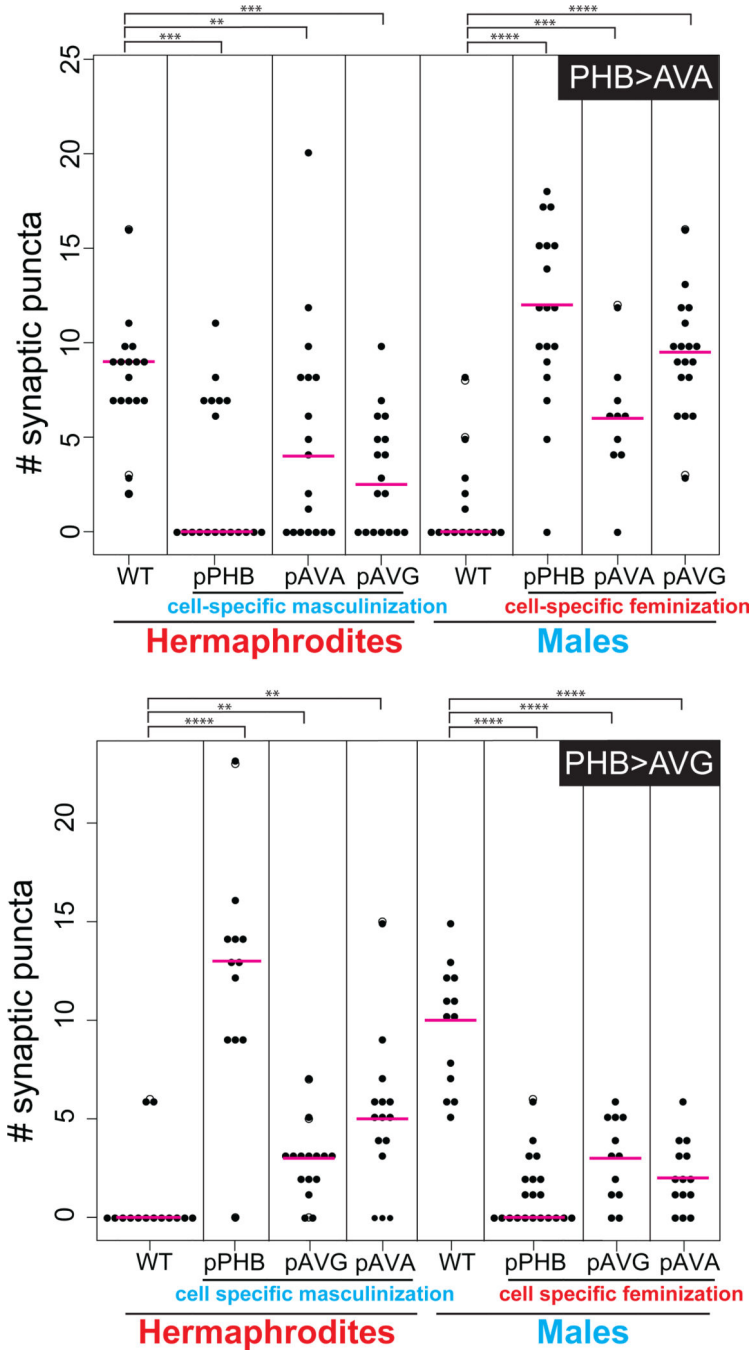

Figure 4. Autonomy and non-autonomy of sex-specific synapse pruning

Either the presynaptic cell (PHB) or the postsynaptic cells (AVA, AVG) were masculinized (by expression of FEM-3) and feminized (by expression of TRA-2^{IC}), and the number of synaptic puncta were quantified in hermaphrodites and males, respectively. We performed the nonparametric Mann-Whitney test (Wilcoxon rank sum test) with Bonferroni correction for multiple comparisons. ****$P < 0.0001$, ***$P < 0.001$, **$P < 0.01$. Magenta horizontal bars represent the median. Results are summarized in Extended Data Fig. 8a. Note that a general trend in the sex-reversal experiments is that the change of the sex of the presynaptic

neuron (PHB) appears to have a stronger effect than changing the sex of either of the postsynaptic cells. Changing the sex of both postsynaptic cells simultaneously did not enhance the effects (Extended Data Fig. 8c).

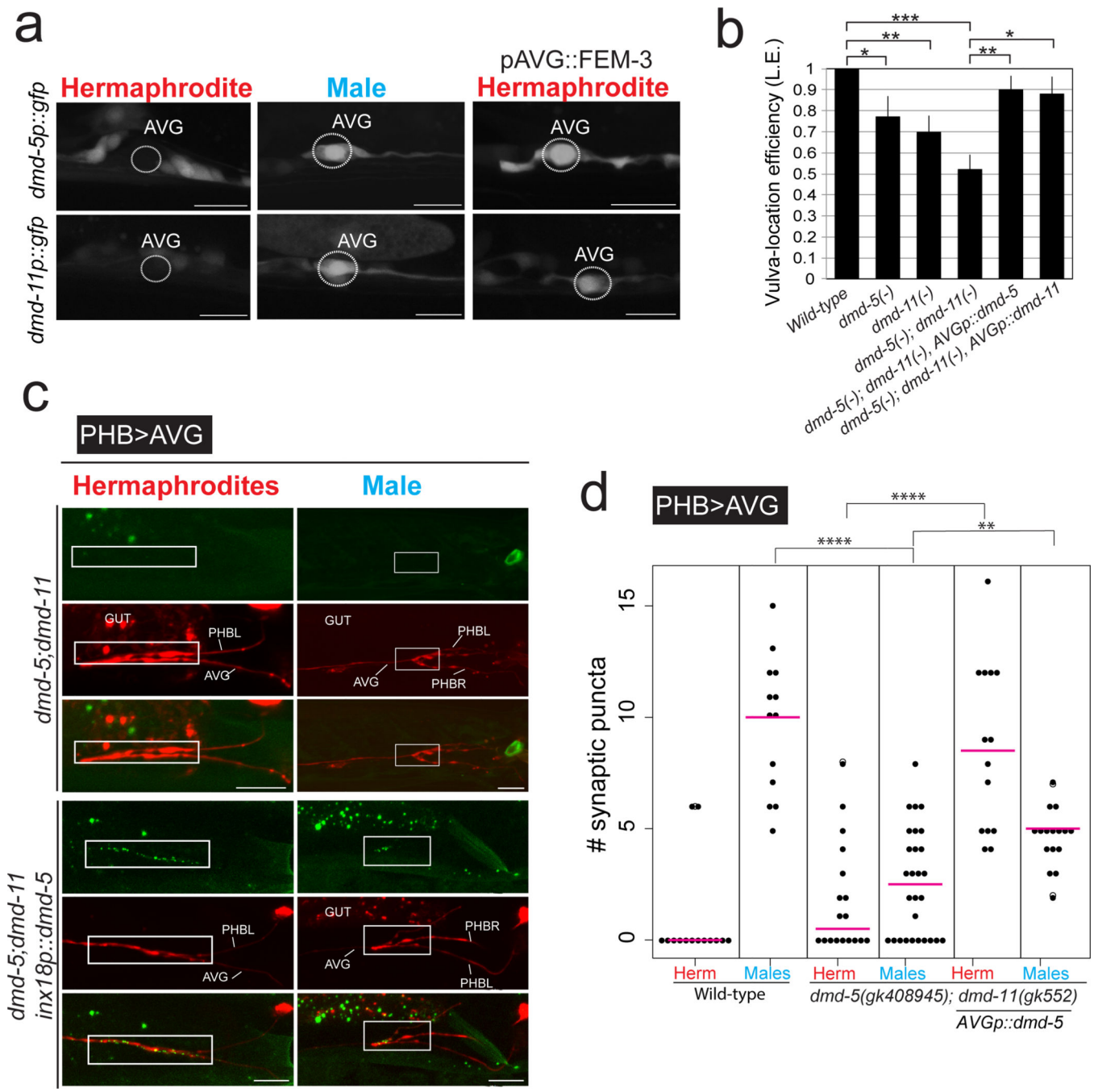

Figure 5. Sexually dimorphic expression and function of *dmd-5* and *dmd-11*

a: Sex-specific expression of *dmd-5* and *dmd-11* reporter genes in AVG. There are no additional dimorphisms in the retrovasicular ganglion, apparent differences are due to differences in z-planes incorporated into the final Z-stack projection. Masculinization of AVG derepresses *dmd-5* and *dmd-11* expression in hermaphrodites AVG. Quantified in Extended Data Figure 9a.

b: Vulva location efficiency is affected in *dmd-5* (n=11)*; dmd-11* (n=20) and *dmd-5;dmd-11* double mutant males (n=29) compared with wild-type males (n=15). Expression of either

dmd-5 (n=10) or *dmd-11* (n=10) in AVG (using the *inx-18* promoter) of double mutant males rescues behavior defects.

c, d:*dmd-5* and *dmd-11* are required for maintenance of AVG synapses. Fluorescent micrographs (**c**) and quantification of synaptic puncta of PHB>AVG (**d**). Region of neurite overlap and observed synaptic puncta marked with white boxes. Quantification of DMD effect on LUA>AVG synapses can be found in Extended Data Fig. 9i. In panels **b, d** we performed the nonparametric Mann-Whitney test (Wilcoxon rank sum test) with Bonferroni correction for multiple comparisons. ****$P < 0.0001$, ***$P < 0.001$, **$P < 0.01$, *$P < 0.05$. Error bars in **b** are S.E.M. Magenta horizontal bars represent the median. Scale bars are 10 μM.